OPEN ACCESS Freely available online

PLoS one

# Dysregulation of Gene Expression in the Artificial Human Trisomy Cells of Chromosome 8 Associated with Transformed Cell Phenotypes

**Hisakatsu Nawata[1], Genro Kashino[2], Keizo Tano[1], Kazuhiro Daino[3], Yoshiya Shimada[3], Hiroyuki Kugoh[4], Mitsuo Oshimura[4], Masami Watanabe[1]***

**1** Laboratory of Radiation Biology, Research Reactor Institute, Kyoto University, Osaka, Japan, **2** Advanced Molecular Imaging Center, Medical School, Oita University, Oita, Japan, **3** Experimental Radiobiology for Children's Health Research Group, Research Center for Radiation Protection, National Institute of Radiological Sciences, Chiba, Japan, **4** Department of Biomedical Science, Institute of Regenerative Medicine and Biofunction, Graduate School of Medical Sciences, Tottori University, Tottori, Japan

## Abstract

A change in chromosome number, known as aneuploidy, is a common characteristic of cancer. Aneuploidy disrupts gene expression in human cancer cells and immortalized human epithelial cells, but not in normal human cells. However, the relationship between aneuploidy and cancer remains unclear. To study the effects of aneuploidy in normal human cells, we generated artificial cells of human primary fibroblast having three chromosome 8 (trisomy 8 cells) by using microcell-mediated chromosome transfer technique. In addition to decreased proliferation, the trisomy 8 cells lost contact inhibition and reproliferated after exhibiting senescence-like characteristics that are typical of transformed cells. Furthermore, the trisomy 8 cells exhibited chromosome instability, and the overall gene expression profile based on microarray analyses was significantly different from that of diploid human primary fibroblasts. Our data suggest that aneuploidy, even a single chromosome gain, can be introduced into normal human cells and causes, in some cases, a partial cancer phenotype due to a disruption in overall gene expression.

**Citation:** Nawata H, Kashino G, Tano K, Daino K, Shimada Y, et al. (2011) Dysregulation of Gene Expression in the Artificial Human Trisomy Cells of Chromosome 8 Associated with Transformed Cell Phenotypes. PLoS ONE 6(9): e25319. doi:10.1371/journal.pone.0025319

**Editor:** Brian P. Chadwick, Florida State University, United States of America

**Received** July 12, 2011; **Accepted** August 31, 2011; **Published** September 29, 2011



**Funding:** This work was supported by grants for Scientific Research from the Ministry of Education, Culture, Sports, Science and Technology of Japan (21310036) and for The Nuclear Safety Research Enhancement Actions from the Nuclear Safety Commission of Japan. A grant from the Central Research Institute of Electric Power Industry also supported part of this work. The funders had no role in study design, data collection and analysis, decision to publish, or preparation of the manuscript.

**Competing Interests:** The authors have declared that no competing interests exist.

* E-mail: msm@rri.kyoto-u.ac.jp

## Introduction

During cell division, errors in chromosomal segregation result in the loss or gain of chromosomes in daughter cells, which is referred to as aneuploidy. An extra or missing chromosome, known as trisomy and monosomy, respectively, is observed in people with developmental disabilities, mental retardation, and cancer. In addition, various types of cancer have karyotypes with complex numerical aberrations [1–3]. Although increasing evidence that aneuploidy is a hallmark of cancer, the causal relationship between aneuploidy and tumorigenesis remains unclear.

The addition of a single chromosome has been reported to have various transcriptional effects in several cell types [4–6]. An increase in the average transcriptional activity of a trisomic chromosome has been observed in trisomic primary mouse cells, human trisomic colorectal cancer cells, immortalized trisomic mammary epithelial cells, and acute myeloid leukemia (AML) cells (with an additional chromosome 8; derived from an AML patient). One chromosome affected not only the gene expression levels on the trisomic chromosome but also a large number of genes on other diploid chromosomes [5]. Apoptosis-regulating genes were significantly down regulated in AML cells containing an additional chromosome 8 that were derived from an AML patient [6].

Despite increased information about the characteristics of aneuploid human cells, the data reported thus far have been obtained from immortalized or cancer-derived cells. Normal human cells have a limited life span and ultimately enter a non-dividing state called senescence [7,8]. It remains unclear whether aneuploidy renders cells immortal or if immortalization induces aneuploidy in cells. To determine the role(s) that aneuploidy plays in human cancer, it will be indispensable to design artificial aneuploid model cells derived from normal human cells.

Trisomy is a simple model of aneuploidy with the gain of a single chromosome. Trisomy of chromosome 8 is the most commonly observed trisomic chromosomal aberration, as has been demonstrated in fibroblastic/myofibroblastic tumors (Fig. S1) [9–12]. In this study, we used normal human diploid embryonic cells (HE35) as a donor for chromosome transfer, and chromosome 8 was chosen as the introduction chromosome. We succeeded in isolation of multiple clones that chromosome 8 became trisomic (trisomy 8 cells). All of the trisomy 8 cells expressed transformed cell-like phenotypes, such as a loss of contact inhibition, regrowth after senescence, and chromosome instability. The overall gene expression profile, determined by microarray analysis, was significantly different from that of the diploid HE35 cells. Our results suggest that aneuploidy is a key factor in tumorigenesis, as demonstrated by disrupted gene expression.

## Results

### Generation of human primary cells bearing three copies of chromosome 8 (trisomy 8 cells)

To generate the trisomy 8 cells, we used microcell-mediated chromosome transfer (MMCT) to introduce an additional chromosome 8 into HE35 cells of culture passage 7, which is a line of normal human diploid primary cells [13]. In this study, inactivated viral envelope proteins of the haemagglutinating virus of Japan (HVJ-E) were used. We isolated three independent clones (HE35tri8-1, -2, and -3) in 35-mm diameter dish, and cultured them by stepwise scale up until reaching confluence in three diameter 100 mm dishes (P100). Then cells were stocked at a total population doubling level of 30 (TPDL 30) for subsequent analysis.

To confirm that the extra chromosome was maintained in each cell clone, we performed Multicolor FISH, which identifies each chromosome by a unique fluorescent color (Fig. 1). The proportion of cells with three copies of chromosome 8 was 90% in HE35tri8-1 and HE35tri8-3 cells and 79% in HE35tri8-2 cells, indicating that each clone had an additional chromosome 8 (Fig. 1).

### Proliferation defects, loss of contact inhibition, and regrowth in the trisomy 8 cells

Aneuploidy causes a proliferative disadvantage in mouse cells [4]. To investigate whether this phenotype could be observed in normal human cells, we examined the proliferative capacity of the artificial trisomy 8 cells in culture. Three artificial trisomy 8 cells had decreased proliferation compared to the diploid HE35 cells (Figs. 2A, S2A–B), indicating that the presence of an additional chromosome inhibits cell proliferation in culture.

Normal cell growth is arrested when cells contact each other in culture and in tissues. This phenomenon, known as contact inhibition, prevents uncontrolled cellular proliferation [14]. In contrast, transformed cells pile densely upon one another [15]. Growth arrest was observed upon cell contact for the normal diploid HE35 cells (Fig. 2B). However, the growth of the trisomy 8 cells (HE35tri8-1, -2, and -3) was not arrested when the cells made contact *in vitro*, and the cells piled densely on one another (Fig. 2B).

Normal human cells undergo a finite number of cell divisions and ultimately enter a non-dividing state called senescence, whereas neither transformed nor cancer cells undergo senescence when they become immortalized. To understand the effects of a single chromosome gain on senescence, we investigated whether the artificial trisomy 8 cells reached senescence and became immortalized. Three clones of normal diploid HE35 (HE35-1, -2, and -4) ultimately entered senescence (Figs. 2C, S3). On the other hand, the trisomy 8 cells (HE35tri8-1, -2, and -3) temporarily exhibited senescence-like characteristics, but after 4–6 weeks of this senescence-like phenotype, a small portion of the trisomy 8 cells had regrown and formed colonies (Figs. 2C and 2D, Table 1). These colonies were made with relatively small sized cells, and the characteristic of the colony morphology, such as piled-up and criss-cross, was the same as those of malignant cells (Fig. 2D). The colony grew up to approximately 5 mm in diameter, but was not able to finally get infinite growth ability.

### DNA damage and chromosomal aberrations

DNA double-strand breaks (DSBs) observed in early tumors initiate genomic instability that leads to cancer [16]. We examined whether DNA DSBs occurred in the trisomy 8 cells (HE35tri8-1, -2, and -3). Previously, both γ-H2AX and 53BP1 were shown to produce foci that co-localized with DSBs [17–20]. There were no differences in the number of foci containing co-localized γ-H2AX and 53BP1 in the trisomy 8 cells and the diploid HE35 cells (Figs. 3A, S4, S5).

Micronucleus assays have emerged as the preferred method to assess chromosome damage because micronuclei provide an index of both chromosome breakage and non-disjunction. Micronuclei are the origin of lagging whole chromosomes and acentric chromosome fragments during anaphase [21]. The micronucleus frequencies were no difference between the trisomy 8 cells and the diploid HE35 cells (Fig. 3B).

Chromosome aberrations are distinctive features of tumors [22]. To investigate whether trisomic conditions bring about chromosome aberrations, we analyzed metaphase chromosome aberrations. Diplochromosomes (chromosomes that have undergone DNA replication but have not segregated) were detected only in the trisomy 8 cells (Table 2, Fig. S6). Chromatid-type aberrations were observed in both the diploid HE35 cells and the trisomy 8 cells, whereas chromosome-type aberrations were found only in the trisomy 8 cells (Table 2). Although the trisomy 8 cells tended to induce both chromosome aberrations and DNA DSBs more than the diploid HE35 cells, there was not the statistical significance.

### Disruption of global gene expression patterns in the trisomy 8 cells

We compared the gene expression profiles of the trisomy 8 cells by microarray analysis. A clustering analysis of genes that exhibited statistically significant changes revealed a pattern that clearly separated the trisomy 8 cells from the diploid HE35 cells (Fig. 4A). The complete dataset is available at the NCBI GEO database (http://www.ncbi.nlm.nih.gov/projects/geo, accession number GSE28076).

The number of genes expressed on each chromosome was examined using a genome-wide transcript expression analysis. Total 127 genes were significantly altered in expression in the trisomy 8 cells compare with the diploid HE35 cells (Table S1). 72% of genes (91 genes) altered in expression were up regulated and the rest (36 genes) were down regulated. We did not yet identify a pathway associated with these genes. The pattern of genes expressed on each chromosome was similar in three clones of the trisomy 8 cells (HE35tri8-1, -2, and -3). The level of genes expressed on trisomic chromosome 8 was increased an average of 115% in each of the trisomy 8 cells compared to those of the diploid HE35 cells (Fig. 4B). In contrast, the average gene expression level on the other chromosomes was significantly decreased (Fig. 4B).

The trisomy 8 cells showed the malignant morphology, which occurs for a decrease of the cell adhesion ability. Therefore, to identify significantly deregulated cell adhesion genes that are involved in the loss of contact inhibition, microarray analyses were performed. As shown in Fig. 4C, Cell adhesion molecule 1 (CADM1) was dramatically down regulated in the trisomy 8 cells. Wilms tumor 1 (WT1), a known oncogene, was markedly up regulated in the trisomy 8 cells (Fig. 4C), but the relationship between WT1 and the phenomena in the trisomy 8 cells remained unclear. Although we have also done the pathway analysis, unfortunately there was no pathway related with 127 genes that changed more than 10 times.

## Discussion

Our analysis of normal human cells containing an additional chromosome 8 (trisomy 8 cells) revealed that all trisomy 8 cells share similar characteristics such as altered gene expression, proliferation defects, loss of contact inhibition, and regrowth after senescence. A small portion of the trisomy 8 cells regrew and formed colonies after

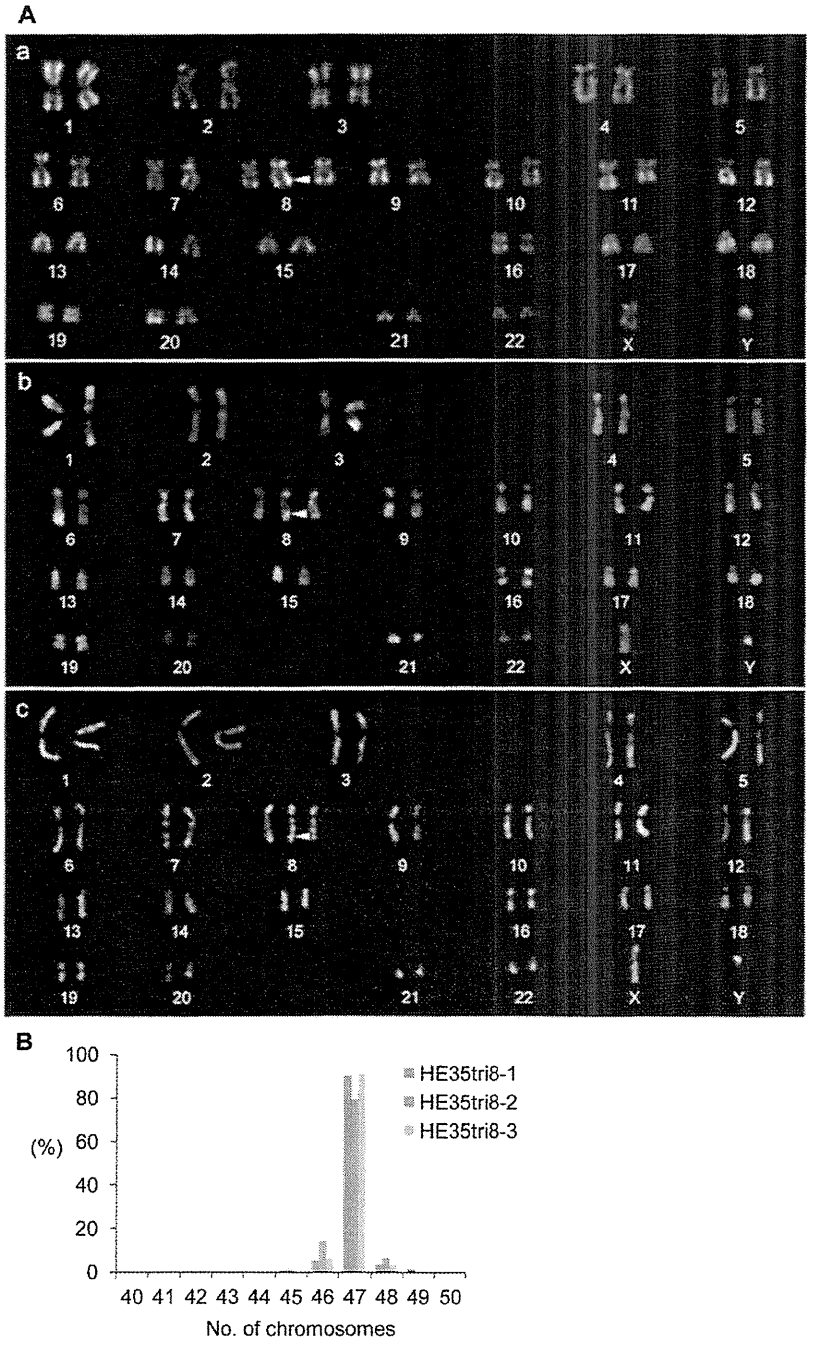


**Figure 1. Generation of trisomic human cells of chromosome 8 (trisomy 8 cells).** (A) Example of a Multicolor FISH analysis of a metaphase spread prepared from HE35tri8-1 at TPDL 30. The arrow indicates the transferred chromosome 8 (the yellow arrow is the neomycin-resistant gene in the transferred chromosome). (B) Chromosome distribution in the trisomy 8 cells.
doi:10.1371/journal.pone.0025319.g001

4–6 weeks of exhibiting a senescence-like state (Figs. 2C–D, Table 1). The trisomy 8 is the most commonly observed chromosome number aberration in fibroblastic/myofibro- blastic tumors (Fig. S1) [9–12]. Transformed cells lose contact inhibition [15] and do not undergo senescence. Our data showed that introducing a chromosome 8 into the normal diploid cells causes expression of transformation-associated phenotypes, such as chromosome instability, and malignant morphological characters. However, all trisomy 8 cells did not finally immortalize. We previously reported that human embryonic cells rapidly deplete telomerase activity associated with the significant shortening of telomeres, and then reached senescence. However, rodent embryo cells retained telomerase activity and the long telomeres (19–50 kb) during the long-term cultures, and cells immortalized. [23,24]. It is likely that

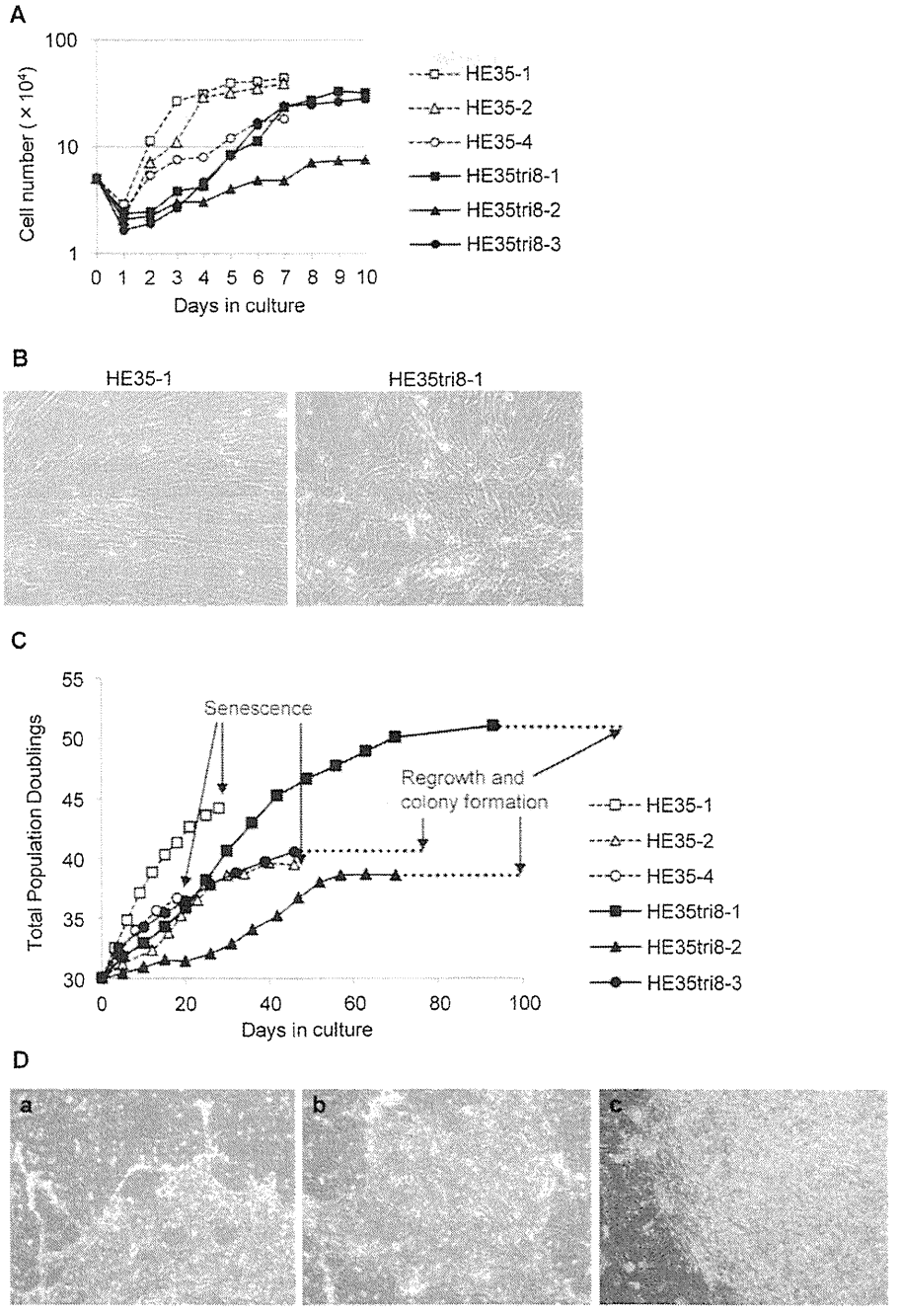


**Figure 2. Proliferation defects, loss of contact inhibition, and regrowth in the trisomy 8 cells.** (A) Proliferation defects in the artificial trisomy 8 cells. The diploid HE35 cells (open squares, open triangles, and open circles) and the trisomy 8 cells (solid squares, solid triangles, and solid circles) were plated and counted daily to detect changes in the cell numbers. (B) Loss of contact inhibition in the trisomy 8 cells (HE35tri8-1 at TPDL 30, HE35-1 at TPDL 30). (C) Cell growth of the cultured diploid HE35 cells and the trisomy 8 cells. (D) A small portion of the trisomy 8 cells regrew and formed colonies after 4–6 weeks of exhibiting a senescence-like state. (D-a) HE35tri8-1 colony, (D-b) HE35tri8-2 colony, (D-c) HE35tri8-3 colony.
doi:10.1371/journal.pone.0025319.g002

trisomy of chromosome 8 might not succeed reactivation of telomerase of human cells. However, unfortunately, because cell number collected from the regrowth colony was too few in the present study, we could not measure telomerase activity yet.

The number of foci where γ-H2AX and 53BP1 co-localized, and micronucleus were no difference between the trisomy 8 cells and the diploid HE35 cells (Fig. 3A–B). However, structural chromosome aberrations were increased in the trisomy 8 cells (Table 2). The number of foci where γ-H2AX and 53BP1 co-localized and the micronucleus frequencies were indirect method of DSB observation, whereas structural chromosome aberrations were direct method. This suggests that the trisomy does not cause

**Table 1.** Frequency of colony formation by regrowth cells after senescence.

| Cells | TPDL[a] | Number of regrowth colony per $1.5\times10^6$ inoculated cells[b] |
|---|---|---|
| HE35-1 | 44.2 | 0 |
| HE35-2 | 39.5 | 0 |
| HE35-4 | 36.7 | 0 |
| HE35tri8-1 | 51.0 | 5.0±2.3 |
| HE35tri8-2 | 38.6 | 3.5±1.9 |
| HE35tri8-3 | 40.6 | 1.0±1.1 |

[a]Total population doubling levels (TPDL) show the number of cell division that cells divided until reaching to senescence.
[b]Frequency of colony formation by regrowth cells in three P100 dishes after senescence. Briefly, $1.5\times10^6$ cells were inoculated into three P100 dishes. Then, cells were incubated in a 100% humidified $CO_2$ incubator at 37°C for 6 weeks with medium change every 3 days. Regrowth colonies were counted. Data show the mean ± S.D. of six independent experiments.
doi:10.1371/journal.pone.0025319.t001

the genetic instability due to DNA DSBs. And also these data suggested that DNA DSB is not a cause of becoming trisomy, but is a result of trisomy.

Diplochromosomes were found only in the trisomy 8 cells, suggesting that trisomy of chromosome 8 causes production of tetraploidy. Although chromatid-type aberrations were seen in both the diploid HE35 cells and the trisomy 8 cells, chromosome-type aberrations were observed in the trisomy 8 cells and not in the diploid HE35 cells. Increased chromosome-type aberrations, but not chromatid-type aberrations, have been associated with an increased cancer risk [25]. The present results revealed that trisomy of chromosome 8 causes other numerical and structural chromosomal aberrations that contribute to the relationship between increased chromosome instability and subsequent cancer risk.

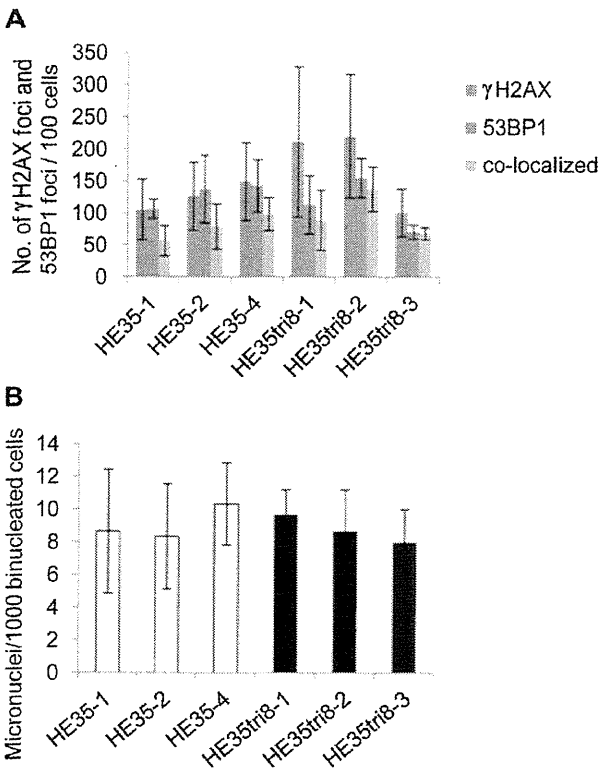


**Figure 3. DNA damage and chromosome aberrations.** (A) Number of γ-H2AX and 53BP1 *foci* in the diploid HE35 cells (HE35-1, -2, and -4) and the trisomy 8 cells (HE35tri8-1, -2, and -3). (B) Micronucleus frequency in the diploid HE35 cells and the trisomy 8 cells.
doi:10.1371/journal.pone.0025319.g003

Previous reports have shown that the average level of gene expression on trisomic chromosomes is increased in mouse cells, human cancer cells, and immortalized human cells compared to diploid cells [4–6]. Our artificial trisomy cells derived from primary human cells had greater average gene expression on the additional chromosome 8 (Fig. 4B). Surprisingly, the average gene expression level on all non-trisomic chromosomes was all decreased; moreover, the profile of each clone was similar (Fig. 4B). Total 127 genes were significantly altered in expression in the trisomy 8 cells compare with the diploid HE35 cells (Table S1). However, it is not clear whether this phenomenon is event that is specific for chromosome 8. The results of our pilot study show that similar change of gene expression is obtained in trisomy of chromosome 1, 6 and 7 (data not shown). These results strongly suggest that gaining even a single chromosome disrupts the expression levels on the trisomic chromosome as well as on the other chromosomes.

Each chromosome occupies a non-random and confined space in the interphase nucleus of higher eukaryotes [26–28]. There is increasing evidence that the positioning of genomic regions in the nuclear space is important for gene regulation [29]. One possible explanation for the general disturbances in the gene expression levels in the trisomy cells is alterations in chromosomal territory.

CADM1 was markedly down regulated in the trisomy 8 cells. The tumor suppressor CADM1 is involved in cell adhesion and is preferentially inactivated in invasive cancers [30–32]. CADM1 is expressed universally in human tissues and is frequently silenced in a variety of human carcinomas [33,34]. A recent study further showed that hypermethylation of the CADM1 promoter induced gene silencing [33,35–40]. We speculate that a down-regulation of the CADM1 gene in the trisomy 8 cells results from hypermethylation of the CADM1 promoter region.

In contrast, WT1 was significantly up regulated in the trisomy 8 cells. The WT1 gene was isolated as the gene responsible for a childhood renal neoplasm, Wilms' tumor, which is thought to arise due to the inactivation of both alleles of the WT1 gene located at chromosome 11p13 [41–43]. The WT1 gene was originally defined as a tumor suppressor gene [41,44–48], but recent studies suggest that the WT1 gene is highly expressed in leukemia and solid tumors and likely plays an oncogenic role in leukemogenesis and tumorigenesis [49,50]. It is possible that aneuploidy results in an epigenetic modification of WT1.

**Table 2.** Frequency of chromosome aberrations in the trisomy 8 cells.

| Cells | Ploidy | No. of cells scored | Chromosome-type aberration (%) | | | Chromatid-type aberration (%) | | | Diplo-chromosome (%) |
|---|---|---|---|---|---|---|---|---|---|
| | | | Gap | Break | Ring | Gap | Break | SU* | |
| HE35-1 | Diploid | 50 | 0 | 0 | 0 | 0 | 0 | 0 | 0 |
| HE35-2 | Diploid | 50 | 0 | 0 | 0 | 0 | 2 | 0 | 0 |
| HE35-4 | Diploid | 50 | 0 | 0 | 0 | 0 | 2 | 0 | 0 |
| HE35tri8-1 | Trisomy 8 | 50 | 2 | 4 | 2 | 0 | 0 | 0 | 6 |
| HE35tri8-2 | Trisomy 8 | 50 | 0 | 2 | 4 | 4 | 0 | 0 | 8 |
| HE35tri8-3 | Trisomy 8 | 50 | 2 | 0 | 0 | 0 | 0 | 2 | 0 |

*Sister Union.

doi:10.1371/journal.pone.0025319.t002

In conclusion, our findings strongly suggest that the addition of a single chromosome causes chromosome instability and extensive disruption of gene expression. Such critical and extensive changes in gene expression can produce parts of transformation-associated phenotypes in aneuploid cells.

## Materials and Methods

### Cells and cell culture

Human embryonic (HE35) cells were obtained from 7- to 8-week-old human embryos previously described [51]. HE35 cells were cultured in Eagle's Minimum Essential Medium (MEM) supplemented with 10% fetal bovine serum at 37°C with 5% $CO_2$ in a humidified environment. The trisomy 8 cells (HE35tri8-1, -2, and -3 cells) were cultured in Eagle's Minimum Essential Medium (MEM) containing 800 μg/ml G418 supplemented with 10% fetal bovine serum at 37°C with 5% $CO_2$ in a humidified environment. Briefly, both the diploid cells derived from HE35 (HE35-1, 2, and 4) and the artificial trisomy 8 cells (HE35tri8-1, -2, and -3) at TPDL 30 were plated at $5\times10^5$ cells per T75 flask. Subconfluent cells were trypsinized and counted to determine the number of cells per T75 flask, and the cells were then replated at $5\times10^5$ cells per T75 flask. Medium change has done every three days of all cultures. This process was repeated until there were either insufficient cells for plating or immortalization (as determined by increased cell proliferation).

### Microcell-mediated chromosome transfer

Donor mouse A9 cells containing human chromosome 8 were established by Kugoh et al. [52]. A9 cells grown in three T-25 flasks at $7\times10^5$ cells/flask in medium containing 800 μg/ml G418 (Nakarai Tesque, Kyoto, Japan). To generate normal human cells containing an additional chromosome 8, we used microcell-mediated chromosome transfer (MMCT) procedure [13]. Briefly, the cells were incubated with 0.05 μg/ml colcemid in medium plus 20% fetal bovine serum for 48 h (to induce micronucleus formation), and then centrifuged in the presence of 10 μg/ml cytochalasin B (Sigma, MO, USA) at 8,000 rpm for 1 h at 34°C to isolate the micronuclei. The micronuclei were then purified by sequentially filtering through sterile filters of pore size 8-, 5-, and 3-μm. The purified micronuclei were suspended in fusion buffer and then HVJ-E was added (Genomone-CF; Ishihara Sangyo, Osaka, Japan) to the recipient cells (HE35 at TPDL7), which were kept on ice for 5 min, and then incubated at 37°C for 15 min. The supernatant was aspirated and MEM containing 800 μg/ml of G418 and 10% FBS was added.

We isolated three independent trisomy 8 cells (HE35tri8-1, -2, and -3) in 35-mm diameter dish (P35), and cells were cultured with doing stepwise scale up using P35, 60-mm diameter dish (P60), and 100-mm diameter dish (P100). Then, cells were cultured until reaching confluence in three P100 dishes. At this point, because total cell number in three dishes is approximately $8\times10^6$, cells of each clone had divided at least 23 times ($8\times10^6\approx2^{23}$) during cloning process. Then, cells were stocked in liquid nitrogen until doing assay. Therefore, cells at 30 TPDL (7PDL+23PDL) were used for subsequent assay.

### Karyotype analysis

To prepare the metaphase chromosome, $5\times10^5$ cells were seeded in P100 dishes. After incubating for 48 h, colcemid (Gibco, CA, USA) was added at a final concentration of 0.06 μg/ml, and the cells were treated for 2 h. Mitotic cells were collected and treated with 0.075 M potassium chloride for 25 min at room temperature. The cells were fixed in Carnoy's solution (methanol: acetic acid, 3:1) and spread on glass slides using the air-drying method. After the cells were stained with a 3% Giemsa solution, the number of chromosomes with at least 50 metaphases per sample was scored.

### Multicolor fluorescence *in situ* hybridization (M-FISH)

Multicolor FISH was performed according to the manufacturer's protocol (Cambio, Cambridge, UK). A chromosome slide was aged on a hot plate at 65°C for 90 min, and the samples were denatured in a solution (70% formamide in 2X SSC) at 65°C for 2 min. After the reaction was quenched in ice-cold 70% ethanol for 4 min, the slides were dehydrated by washing for 5 min each in 70% ethanol and 100% ethanol and then dried at 37°C. An aliquot (10 ml) of the M-FISH probes was denatured at 65°C for 10 min and applied to the chromosome slide. Hybridization was performed at 37°C for 48 h in a humidified atmosphere. After hybridization, each slide was washed twice for 5 min each in washing solution (50% formamide in 0.5X SSC) at 45°C, followed by two incubations of 5 min each in 1X SSC at 45°C. Each slide was then incubated for 4 min in detergent washing solution (0.05% detergent DT in 4X SSC) at 45°C. An aliquot (125 ml) of the detection reagent was applied to the slides, which were then covered with parafilm and subsequently incubated in a humidified atmosphere for 20 min at 37°C. After the parafilm was removed, the slides were washed three times for 4 min in detergent washing solution at room temperature. Finally, the DNA was stained with 4′, 6-diamino-2-phenylindole (DAPI) in antifade solution. Chromosome images were captured and analyzed using the Leica CW4000 system.

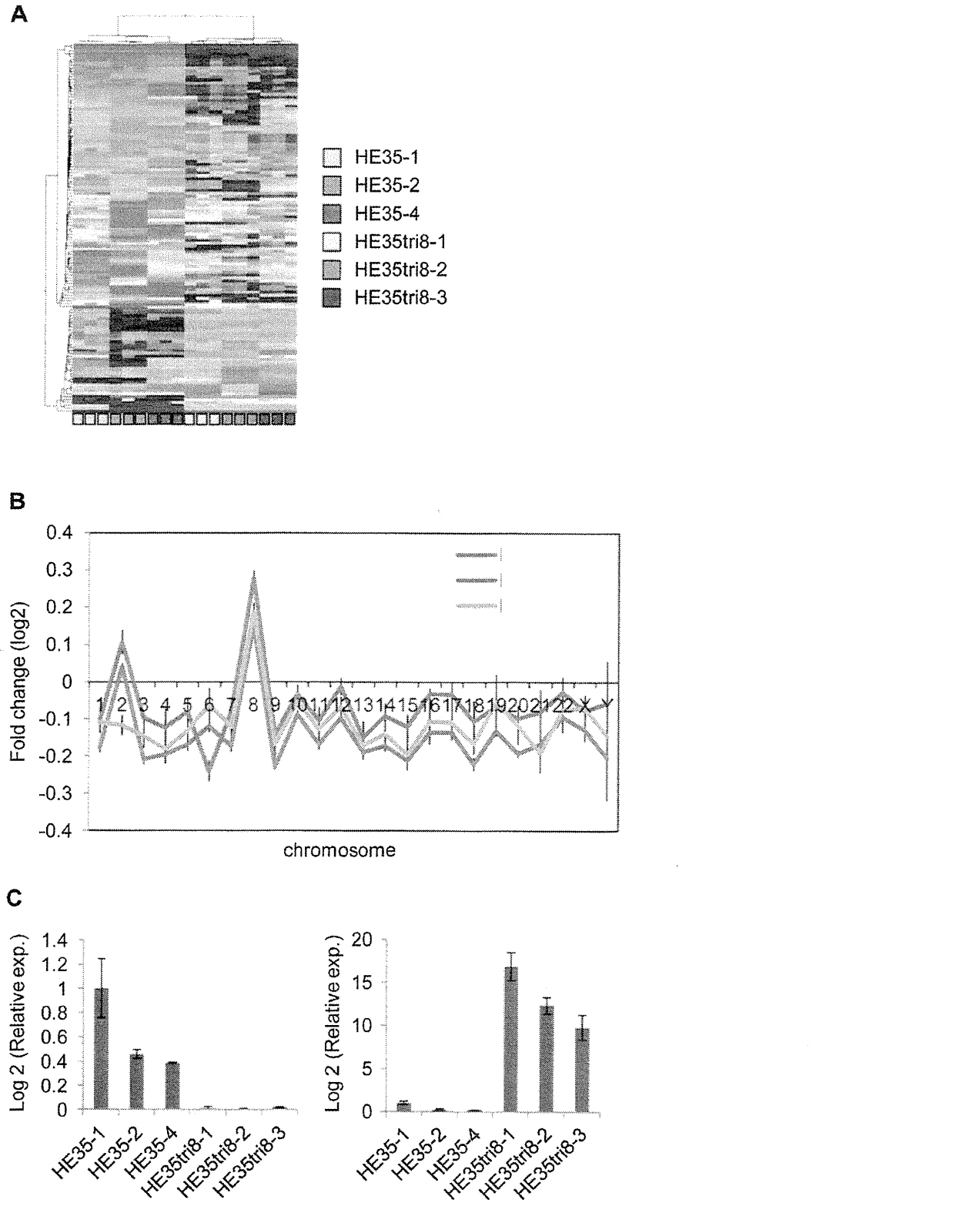


**Figure 4. Disruption of the global gene expression patterns in the trisomy 8 cells.** (A) Clustering analysis of 127 genes that exhibited statistically significant changes in the trisomy 8 cells (HE35tri8-1, -2, and -3) versus the diploid HE35 cells (HE35-1, -2, and -4). Three independent experiments were performed for each clone. (B) Average gene expression pattern by chromosome. The average chromosome expression ratios relative to the same reference RNA pool for each trisomy 8 cells was then normalized to the average of the ratio value for the diploid HE35 cells. (C) CADM1 (11q23.2) and WT1 (11p13) gene expression in the trisomy 8 cells (HE35tri8-1, -2, and -3) and the diploid HE35 cells (HE35-1, -2, and -4).
doi:10.1371/journal.pone.0025319.g004

### Proliferation assay

Exponentially growing diploid HE35 cells (HE35-1, -2, and -4) at TPDL 37 and the trisomy 8 cells (HE35tri8-1, -2, and -3) at TPDL 37 were plated at a density of $5\times10^4$ cells in individual wells of multiple 6-well plates. All cells were plated in a final volume of 3 ml of medium. Cells were incubated in humidified 5% $CO_2$ incubator at 37°C. The medium was replaced with fresh medium every three days throughout the experiment. Cells were harvested by trypsinization and cell number was counted by hemocytometer every day.

### Senescence-associated β-galactosidase assay

Cells were washed once with $Ca^{2+}$- and $Mg^{2+}$-free phosphate-buffered saline ($PBS^-$) and fixed in a 0.2% paraformaldehyde solution containing 0.2% glutaraldehyde for 5 min at room temperature. After washing with $PBS^-$, the fixed cells were incubated in SA-β-gal staining solution (40 mM citric acid/sodium phosphate, pH 6.0, 5 mM potassium ferrocyanide, 5 mM potassium ferricyanide, 150 mM NaCl, and 2 mM $MgCl_2$) containing 1 mg/ml 5-bromo-4-chloro-3-indolylβ-D-galactopyranoside (X-gal) to stain senescent cells.

### Immunofluorescence detection

Both the diploid HE 35 cell and the trisomy 8 cells at TPDL 37 were fixed in 4% formaldehyde in $PBS^-$ for 15 min, permeabilized for 10 min on ice in 0.5% Triton X-100 in $PBS^-$, and then washed extensively with $PBS^-$. Then, the coverslips were incubated with anti-phosphorylated histone H2AX at serine 139 (Upstate Biotechnology, NY, USA) and 53BP1 (Bethyl Laboratory, TX, USA) in TBS-DT (20 mM Tris-HCl, 137 mM NaCl, pH 7.6, containing 50 mg/ml skim milk and 0.1% Tween-20) for 2 h at 37°C. The primary antibodies were washed with $PBS^-$, and Alexa Fluor 488–labeled anti-mouse IgG antibody and Alexa Fluor 594–labeled anti-rabbit *IgG* antibody (Molecular Probes, CA, USA) was added. The coverslips were incubated for 1 h at 37°C, washed with $PBS^-$, and sealed on glass slides with 0.05 ml of $PBS^-$ containing 10% glycerol. The cells were examined by fluorescence microscopy.

### Micronucleus assay

Cells at TPDL 37 were treated with 2 μg/ml cytochalasin B for 24 h in a T25 flask. They were then harvested and treated with 3 ml of hypotonic (0.1 M) KCl for 20 min, and fixed with 3 ml of methanol/acetic acid (5:1). The cell suspensions were centrifuged at 1,200 rpm for 5 min. Then, the cells were suspended in 4 ml methanol/acetic acid solution and incubated on ice for 5 min. After centrifugation, the supernatant was removed and a 0.5–1 ml methanol/acetic acid solution was added to the cells. The cell suspensions were dropped onto slides and stained with 7.5% Giemsa for 40 min. The number of micronuclei per 1,000 binucleated cells was counted.

### Transcript array and date analysis

RNA was isolated from cells at TPDL 37 using an RNeasy Mini Kit (Qiagen, Tokyo, Japan). Five hundred nanograms of total RNA was then reverse-transcribed and labeled with a Quick Amp Labeling Kit, as recommended by the manufacturer (Agilent Technologies, CA, USA) and hybridized to Human Whole Genome Arrays (Agilent Technologies, CA, USA). Chips were analyzed and the data were extracted for examination using GeneSpring GX 11.5 Software (Agilent Technologies, CA, USA). To identify significantly related genes, GeneSpring GX 11.5 was used to perform a *t*-test.

### Accession number

The microarray data reported herein are available at the NCBI GEO database (http://www.ncbi.nlm.nih.gov/projects/geo, accession number GSE28076).

## Supporting Information

**Figure S1** The distribution of trisomy in fibroblastic/myofibroblastic tumors (all sub types). The Mitelman Database of Chromosome Aberrations in Cancers was used as a source of the data (http://cgap.nci.nih.gov/Chromosomes/Mitelman).
(TIF)

**Figure S2** The daily behavior of a culture of normal human cells (diploid HE35-1) and of a culture of the artificial trisomy 8 cells (HE35tri8-3) in the same region of culture. (A) normal human cells (diploid HE35-1), (B) artificial trisomy 8 cells (HE35tri8-3).
(TIF)

**Figure S3** Senescence-associated β-galactosidase staining was altered in cultures of the diploid HE35 cells (HE35-1, -2, and -4). β-galactosidase staining is shown in blue.
(TIF)

**Figure S4** The diploid HE35 cells (HE35-1, -2, and -4) were coimmunostained with anti-γ-H2AX and anti-53BP1 antibodies.
(TIF)

**Figure S5** The trisomy 8 cells (HE35tri8-1, -2, and -3) were coimmunostained with anti-γ-H2AX and anti-53BP1 antibodies.
(TIF)

**Figure S6** Diplochromosomes at metaphase in the trisomy 8 cell (HE35tri8-1).
(TIF)

**Table S1** The gene number that an expression level was significantly changed by a chromosome 8 introduction.
(TIFF)

## Author Contributions

Conceived and designed the experiments: MW HN GK KT KD YS HK MO. Performed the experiments: MW HN GK KT KD YS HK MO. Analyzed the data: MW HN GK KT KD YS HK MO. Contributed reagents/materials/analysis tools: MW HN GK KT KD YS HK MO. Wrote the paper: MW HN GK KT KD YS HK MO.

## References


1. Ganmore I, Smooha G, Izraeli S (2009) Constitutional aneuploidy and cancer predisposition. Hum Mol Genet 18: R84–93.
2. Weaver BAA, Cleveland DW (2006) Does aneuploidy cause cancer? Current Opinion in Cell Biology 18: 658–667.
3. Hassold T, Hunt P (2001) To err (meiotically) is human: the genesis of human aneuploidy. Nat Rev Genet 2: 280–291.
4. Williams BR, Prabhu VR, Hunter KE, Glazier CM, Whittaker CA, et al. (2008) Aneuploidy Affects Proliferation and Spontaneous Immortalization in Mammalian Cells. Science 322: 703–709.
5. Upender MB, Habermann JK, McShane LM, Korn EL, Barrett JC, et al. (2004) Chromosome transfer induced aneuploidy results in complex dysregulation of the cellular transcriptome in immortalized and cancer cells. Cancer Res 64: 6941–6949.
6. Virtaneva K, Wright FA, Tanner SM, Yuan B, Lemon WJ, et al. (2001) Expression profiling reveals fundamental biological differences in acute myeloid leukemia with isolated trisomy 8 and normal cytogenetics. Proc Natl Acad Sci U S A 98: 1124–1129.
7. Shay JW, Wright WE (2000) Hayflick, his limit, and cellular ageing. Nat Rev Mol Cell Biol 1: 72–76.
8. Hayflick L, Moorhead PS (1961) The serial cultivation of human diploid cell strains. Exp Cell Res 25: 585–621.
9. Fletcher JA, Naeem R, Xiao S, Corson JM (1995) Chromosome aberrations in desmoid tumors trisomy 8 may be a predictor of recurrence. Cancer Genetics and Cytogenetics 79: 139–143.
10. Schofield DE, Fletcher JA, Grier HE, Yunis EJ (1994) Fibrosarcoma in Infants and Children: Application of New Techniques. The American Journal of Surgical Pathology 18: 14–24.

11. Schofield DE, Yunis EJ, Fletcher JA (1993) Chromosome aberrations in mesoblastic nephroma. Am J Pathol 143: 714–724.
12. Sankary S, Dickman PS, Wiener E, Robichaux W, Swaney WP, et al. (1993) Consistent numerical chromosome aberrations in congenital fibrosarcoma. Cancer Genetics and Cytogenetics 65: 152–156.
13. Doherty AM, Fisher EM (2003) Microcell-mediated chromosome transfer (MMCT): small cells with huge potential. Mamm Genome 14: 583–592.
14. Fagotto F, Gumbiner BM (1996) Cell Contact-Dependent Signaling. Developmental Biology 180: 445–454.
15. Perucho M, Goldfarb M, Shimizu K, Lama C, Fogh J, et al. (1981) Human-tumor-derived cell lines contain common and different transforming genes. Cell 27: 467–476.
16. Bartkova J, Horejsi Z, Koed K, Kramer A, Tort F, et al. (2005) DNA damage response as a candidate anti-cancer barrier in early human tumorigenesis. Nature 434: 864–870.
17. Fernandez-Capetillo O, Chen H-T, Celeste A, Ward I, Romanienko PJ, et al. (2002) DNA damage-induced G2-M checkpoint activation by histone H2AX and 53BP1. Nat Cell Biol 4: 993–997.
18. Rappold I, Iwabuchi K, Date T, Chen J (2001) Tumor Suppressor P53 Binding Protein 1 (53bp1) Is Involved in DNA Damage–Signaling Pathways. The Journal of Cell Biology 153: 613–620.
19. Schultz LB, Chehab NH, Malikzay A, Halazonetis TD (2000) p53 binding protein 1 (53BP1) is an early participant in the cellular response to DNA double-strand breaks. J Cell Biol 151: 1381–1390.
20. Rogakou EP, Pilch DR, Orr AH, Ivanova VS, Bonner WM (1998) DNA Double-stranded Breaks Induce Histone H2AX Phosphorylation on Serine 139. Journal of Biological Chemistry 273: 5858–5868.
21. Fenech M (2000) The in vitro micronucleus technique. Mutation Research/Fundamental and Molecular Mechanisms of Mutagenesis 455: 81–95.
22. Solomon E, Borrow J, Goddard A (1991) Chromosome aberrations and cancer. Science 254: 1153–1160.
23. Yang Z, Kodama S, Suzuki K, Watanabe M (1998) Telomerase activity, telomere length, and chromosome aberrations in the extension of life span of human embryo cells induced by low-dose X-rays. J Radiat Res (Tokyo) 39(1): 35–51.
24. Kodama S, Mori I, Roy K, Yang Z, Suzuki K, Watanabe M (2001) Culture condition-dependent senescence-like growth arrest and immortalization in rodent embryo cells. Radiat Res 155(1 Pt 2): 254–262.
25. Boffetta P, van der Hel O, Norppa H, Fabianova E, Fucic A, et al. (2007) Chromosomal Aberrations and Cancer Risk: Results of a Cohort Study from Central Europe. American Journal of Epidemiology 165: 36–43.
26. Meaburn KJ, Misteli T (2007) Cell biology: Chromosome territories. Nature 445: 379–381.
27. Lanctot C, Cheutin T, Cremer M, Cavalli G, Cremer T (2007) Dynamic genome architecture in the nuclear space: regulation of gene expression in three dimensions. Nat Rev Genet 8: 104–115.
28. Fraser P, Bickmore W (2007) Nuclear organization of the genome and the potential for gene regulation. Nature 447: 413–417.
29. Gasser SM (2002) Visualizing Chromatin Dynamics in Interphase Nuclei. Science 296: 1412–1416.
30. Murakami Y (2005) Involvement of a cell adhesion molecule, TSLC1/IGSF4, in human oncogenesis. Cancer Science 96: 543–552.
31. Goto A, Niki T, Chi-pin L, Matsubara D, Murakami Y, et al. (2005) Loss of TSLC1 expression in lung adenocarcinoma: Relationships with histological subtypes, sex and prognostic significance. Cancer Science 96: 480–486.
32. Kuramochi M, Fukuhara H, Nobukuni T, Kanbe T, Maruyama T, et al. (2001) TSLC1 is a tumor-suppressor gene in human non-small-cell lung cancer. Nat Genet 27: 427–430.
33. Mao X, Seidlitz E, Truant R, Hitt M, Ghosh HP (2004) Re-expression of TSLC1 in a non-small-cell lung cancer cell line induces apoptosis and inhibits tumor growth. Oncogene 23: 5632–5642.
34. Shingai T, Ikeda W, Kakunaga S, Morimoto K, Takekuni K, et al. (2003) Implications of Nectin-like Molecule-2/IGSF4/RA175/SgIGSF/TSLC1/Syn-CAM1 in Cell-Cell Adhesion and Transmembrane Protein Localization in Epithelial Cells. Journal of Biological Chemistry 278: 35421–35427.
35. Sakurai-Yageta M, Masuda M, Tsuboi Y, Ito A, Murakami Y (2009) Tumor suppressor CADM1 is involved in epithelial cell structure. Biochemical and Biophysical Research Communications 390: 977–982.
36. Tsujiuchi T, Sugata E, Masaoka T, Onishi M, Fujii H, et al. (2007) Expression and DNA methylation patterns of Tslc1 and Dal-1 genes in hepatocellular carcinomas induced by N-nitrosodiethylamine in rats. Cancer Science 98: 943–948.
37. Shimizu K, Onishi M, Sugata E, Fujii H, Honoki K, et al. (2007) Aberrant DNA methylation of the 5′ upstream region of Tslc1 gene in hamster pancreatic tumors. Biochemical and Biophysical Research Communications 353: 522–526.
38. Heller G, Fong KM, Girard L, Seidl S, End-Pfutzenreuter A, et al. (2005) Expression and methylation pattern of TSLC1 cascade genes in lung carcinomas. Oncogene 25: 959–968.
39. Ito T, Shimada Y, Hashimoto Y, Kaganoi J, Kan T, et al. (2003) Involvement of TSLC1 in Progression of Esophageal Squamous Cell Carcinoma. Cancer Research 63: 6320–6326.
40. Fukami T, Fukuhara H, Kuramochi M, Maruyama T, Isogai K, et al. (2003) Promoter methylation of the TSLC1 gene in advanced lung tumors and various cancer cell lines. International Journal of Cancer 107: 53–59.
41. Algar EM, Kenney MT, Simms LA, Smith SI, Kida Y, et al. (1995) Homozygous intragenic deletion in the WT1 gene in a sporadic Wilms' tumour associated with high levels of expression of a truncated transcript. Hum Mutat 5: 221–227.
42. Gessler M, Poustka A, Cavenee W, Neve RL, Orkin SH, et al. (1990) Homozygous deletion in Wilms tumours of a zinc-finger gene identified by chromosome jumping. Nature 343: 774–778.
43. Call KM, Glaser T, Ito CY, Buckler AJ, Pelletier J, et al. (1990) Isolation and characterization of a zinc finger polypeptide gene at the human chromosome 11 Wilms' tumor locus. Cell 60: 509–520.
44. Loeb D, Sukumar S (2002) The Role of WT1 in Oncogenesis: Tumor Suppressor or Oncogene? International Journal of Hematology 76: 117–126.
45. Little M, Wells C (1997) A clinical overview of WT1 gene mutations. Human Mutation 9: 209–225.
46. Rauscher F (1993) The WT1 Wilms tumor gene product: a developmentally regulated transcription factor in the kidney that functions as a tumor suppressor. The FASEB Journal 7: 896–903.
47. Haber DA, Park S, Maheswaran S, Englert C, Re GG, et al. (1993) WT1-mediated growth suppression of Wilms tumor cells expressing a WT1 splicing variant. Science 262: 2057–2059.
48. Coppes M, Campbell C, Williams B (1993) The role of WT1 in Wilms tumorigenesis. The FASEB Journal 7: 886–895.
49. Huff V (2011) Wilms' tumours: about tumour suppressor genes, an oncogene and a chameleon gene. Nat Rev Cancer 11: 111–121.
50. Sugiyama H (2010) WT1 (Wilms' tumor gene 1): biology and cancer immunotherapy. Jpn J Clin Oncol 40: 377–387.
51. Suzuki M, Yang Z, Nakano K, Yatagai F, Suzuki K, et al. (1998) Extension of in vitro life-span of gamma-irradiated human embryo cells accompanied by chromosome instability. J Radiat Res (Tokyo) 39: 203–213.
52. Kugoh H, Mitsuya K, Meguro M, Shigenami K, Schulz TC, Oshimura (1999) Mouse A9 cells containing single human chromosomes for analysis of genomic imprinting. DNA Res 6: 165–172.

DNA Repair 10 (2011) 915–925

Contents lists available at ScienceDirect

DNA Repair

journal homepage: www.elsevier.com/locate/dnarepair

# The Rev1 translesion synthesis polymerase has multiple distinct DNA binding modes

Frederik H. de Groote[a], Jacob G. Jansen[b], Yuji Masuda[c], Dipen M. Shah[a], Kenji Kamiya[c], Niels de Wind[b], Gregg Siegal[a,*]

[a] Department of Protein Chemistry, Leiden Institute of Chemistry, Gorlaeus Laboratory, P.O. Box 9502, 2300 RA Leiden, The Netherlands
[b] Department of Toxicogenetics, Leiden University Medical Center, Postal Zone S4-P, P.O. Box 9600, 2300 RC Leiden, The Netherlands
[c] Research Institute for Radiation Biology and Medicine, Hiroshima University, 1-2-3 Kasumi, Minamiku, Hiroshima 734-8553, Japan

ARTICLE INFO

*Article history:*
Received 12 January 2011
Received in revised form 25 March 2011
Accepted 27 April 2011
Available online 12 July 2011

*Keywords:*
Trans-lesion synthesis
Rev1
DNA binding

ABSTRACT

Rev1 is a eukaryotic DNA polymerase of the Y family involved in translesion synthesis (TLS), a major damage tolerance pathway that allows DNA replication at damaged templates. Uniquely amongst the Y family polymerases, the N-terminal part of Rev1, dubbed the BRCA1 C-terminal homology (BRCT) region, includes a BRCT domain. While most BRCT domains mediate protein–protein interactions, Rev1 contains a predicted α-helix N-terminal to the BRCT domain and in human Replication Factor C (RFC) such a BRCT region endows the protein with DNA binding capacity. Here, we studied the DNA binding properties of yeast and mouse Rev1. Our results show that the BRCT region of Rev1 specifically binds to a 5′ phosphorylated, recessed, primer–template junction. This DNA binding depends on the extra α-helix, N-terminal to the BRCT domain. Surprisingly, a stretch of 20 amino acids N-terminal to the predicted α-helix is also critical for high-affinity DNA binding. In addition to 5′ primer–template junction binding, Rev1 efficiently binds to a recessed 3′ primer–template junction. These dual DNA binding characteristics are discussed in view of the proposed recruitment of Rev1 by 5′ primer–template junctions, downstream of stalled replication forks.



## 1. Introduction

Advancing replication forks may stall at DNA lesions due to the inability of the high fidelity polymerases δ and ε to accommodate modified nucleotides in their active sites. If not resolved, these stalled forks can collapse, resulting in chromosomal breakage or inappropriate cell death. Stalled replication forks can be rescued by a DNA damage tolerance pathway called DNA translesion synthesis (TLS) [1,2]. In TLS, the high fidelity replicative polymerase (pol) is replaced by a specialized, low fidelity pol that synthesizes a short stretch of DNA past the site of damage. The active site of the low fidelity pol is generally much more open than that of the replicative pols thereby accommodating bulky adducts or abasic sites in the damaged DNA strand. It is thought that in eukaryotes TLS occurs *via* the action of two polymerases, typically one of the Y family pols Rev1, η, ι or κ [1] and polζ, a B family pol that efficiently extends mismatched primers. TLS is a double-edged sword in that it allows the completion of genomic replication and yet is responsible for introducing the majority of DNA damage-induced mutations [3]. It is therefore clear that a high level of regulation must occur to ensure that only the optimal pol can access the 3′ terminus and carry out TLS.

Rev1 is a unique member of the Y family pols since its catalytic activity is limited to DNA-dependent, deoxycytidyl transferase activity [4], in particular opposite abasic sites and a variety of different types of adducted guanines [5]. Rev1 is responsible for the majority of DNA damage-induced mutagenesis and is involved in the generation of resistance to the anticancer drug cisplatin [6]. However, the polymerase activity is not essential for most mutagenic TLS mediated by Rev1. For example, in contrast to complete loss of Rev1 that leads to a hypomutable phenotype, a mutant Rev1 protein lacking a functional catalytic domain does not lead to a change in TLS activity or in mutation frequencies, although incorporation of dCMP was abolished [5,7]. Therefore, it is believed that the polymerase activity of Rev1 is only required for certain types of DNA damage [1]. Conversely, mutations outside of the catalytic domain have dramatic effects on bypass of a broad range of DNA damage [5,8].

*Abbreviations:* aa, amino acids; BRCT, BRCA1 C-terminal homology; CIP, calf intestinal phosphatase; ds, double stranded; EMSA, Electrophoretic Mobility Shift Assay; mm, *Mus musculus*; PCNA, proliferating cell nuclear antigen; PMSF, phenylmethylsulfonyl fluoride; pol, DNA polymerase; RFC, Replication Factor C; sc, *Saccharomyces cerevisiae*; ss, single stranded; TLS, translesion synthesis; UBMs, ubiquitin binding motifs.

* Corresponding author. Tel.: +31 71 527 4543; fax: +31 71 527 4609.
*E-mail address:* g.siegal@chem.leidenuniv.nl (G. Siegal).

1568-7864/$ – see front matter © 2011 Elsevier B.V. All rights reserved.
doi:10.1016/j.dnarep.2011.04.033

In addition to the deoxycytidyl transferase domain, mammalian Rev1 includes three other functional domains: an N-terminal BRCA1 C-terminal homology (BRCT) domain, two ubiquitin binding motifs (UBMs) and a C-terminal region that binds to other Y family pols and polζ [1,9]. The latter is in agreement with a proposed regulatory role of Rev1 in the selection of other Y family pols and recruitment of polζ to template lesions during TLS. The UBMs mediate binding of Rev1 to mono-ubiquitinated PCNA which is produced in response to DNA damaging agents such as ultraviolet (UV) light [10,11]. This association with ubiquitinated PCNA is responsible for the localization of Rev1 into repair foci upon DNA damage induction. BRCT domains comprise a large superfamily and are mainly found in proteins involved in DNA repair or cell cycle checkpoints [12,13]. The majority of the BRCT domains mediate a range of protein–protein interactions including homo-dimerization, hetero-dimerization with, and without, other BRCT domains and phosphopeptide binding (reviewed in [14]). Although the BRCT domain of Rev1 is not essential for survival after exposure to many DNA-damaging agents, mutations in this domain strongly reduce Rev1-dependent mutagenesis in yeast and mammals [5,15,16]. This indicates that the BRCT domain of Rev1 plays an important role in the regulation of TLS.

A molecular mechanism for the biological function of the Rev1 BRCT domain remains elusive. It has been suggested that the BRCT domain of Rev1 is required for efficient binding of Rev1 to the processivity clamp PCNA [17] and the Rev7 subunit of polζ, the latter in conjunction with a C-terminal region [18]. In addition, the BRCT domain is responsible for localization of Rev1 to sites of (presumably stalled) DNA replication in the absence of induced damage [19] and to double strand DNA breaks [20].

Recently, we have suggested a role for vertebrate Rev1 in filling of post-replicative gaps that oppose damaged nucleotides [21], in addition to a proposed role in direct lesion bypass [22]. Post-replicative gap filling has been proposed as a mechanism that converts relatively small DNA strands into DNA of high molecular weight in replicating bacteria and eukaryotic cells exposed to UV light [23–26]. We have suggested a model in which the 5′ end of a primer–template junction at a post-replicative gap acts as a docking site for Rev1 [27]. Subsequently, Rev1 may migrate to the 3′ end of the stalled replication fork to mediate gap filling TLS [28].

In this work we set out to define the DNA binding properties of Rev1, in particular of the N-terminal BRCT region. In our recent study on the DNA binding properties of the BRCT region of the large subunit of human Replication Factor C (RFC), we observed that binding to recessed 5′-phosphorylated ends in dsDNA does not only depend on the BRCT domain itself, but also depends on additional amino acids flanking it [29]. In the same study, we noted that Rev1 exhibited sequence similarity with the BRCT region of RFC [29]. Here we show that Rev1 from divergent species preferentially binds to the recessed 5′ phosphorylated terminus of dsDNA and that this binding requires the conserved BRCT domain, as well as residues N terminal to the BRCT domain. Additionally, Rev1 displays BRCT domain-independent binding to a 3′ OH primer–template junction and, transiently, to single-stranded DNA. Our studies support a role of the Rev1 BRCT region in recruitment of Rev1 to 5′ primer–template junctions at post-replicative gaps.

## 2. Materials and methods

### 2.1. Construction of Rev1 expression plasmids

DNA fragments encoding amino acids 1–131 (mRev1(1–131)), 21–131 (mRev1(21–131)) and 41–131 (mRev1(41–131)) of mouse Rev1 were amplified by PCR and cloned into a pET20b plasmid for bacterial expression. A DNA fragment encoding amino acids 1–251 of yeast Rev1 was PCR amplified and inserted into the bacterial expression vector pET20b in an identical manner. All PCR products were digested with NdeI and XhoI and ligated with pET20b, treated with the same restriction enzymes, to give respectively pET20bmRev1(1–131), pET20bmRev1(21–131), pET20bmRev1(41–131) and pET20bscRev1(1–251). Each construct contained a non-encoded methionine at the N-terminus and a 6 his affinity tag at the C-terminus. All constructs were verified by sequence analysis.

### 2.2. Site-directed mutagenesis

A two step, whole plasmid PCR was performed using pET20bmRev1(1–131) as template. In the first PCR reaction forward primers containing the desired point mutation were used in combination with a reverse primer, containing a BamHI site, to copy one half of the plasmid, yielding product A. To copy the second half of the plasmid, reverse primers complementary to the forward primers used in the first reaction, were used in a second PCR reaction in combination with a forward primer, which also contained a BamHI site, yielding product B. Both products were incubated with DpnI, purified and used as template in a third PCR reaction yielding the linear plasmid containing the specific point mutations. Purified PCR products were digested with BamHI, and subsequently ligated into the pET20b expression vector using T4 DNA ligase. All mutants were sequenced to verify the presence of the desired mutation and the absence of any unintentionally induced ones.

### 2.3. Expression and purification of Rev1 protein fragments

BL21 pLySs cells (Novagen) were transformed with the pET20bmRev1 containing either wild type or mutant sequences or pET20bscRev1(1–251) plasmids and cultured in LB medium containing ampicillin (50 μg/ml) and chloramphenicol (34 μg/ml) at 25 °C. Protein expression was induced at an $OD_{600}$ of 0.6 with 1 mM IPTG and growth was continued overnight at 18 °C. Cells were collected by centrifugation at 5000 rpm for 20 min. The cell pellets were resuspended in binding buffer containing 20 mM Tris–HCl (pH 7.5), 5 mM Imidazole and 500 mM NaCl, and stored at −80 °C.

Cells were thawed on ice and subsequently lysed by passage through a French press at 1500 psig twice. The recovered lysate was centrifuged at 35,000 rpm and 4 °C for 45 min using a Beckman Ti35 rotor. The supernatant was applied to a 5 ml HisTrap HP $Ni^{2+}$ chelating column (GE healthcare) equilibrated in the manufacturer's suggested binding buffer supplemented with PMSF. The column was washed with 20 mM Tris–HCl (pH 7.9); 60 mM Imidazole and 500 mM NaCl and protein was eluted with 20 mM Tris–HCl (pH 7.9); 500 mM Imidazole and 500 mM NaCl.

The eluted fraction was diluted to a final concentration of 250 mM NaCl by adding 25 mM Tris–HCl (pH 7.9), and applied to a 5 ml SP ion exchange column (GE healthcare) equilibrated in 25 mM HEPES (pH 7.5); 50 mM NaCl and 1 mM DTT, followed by elution using a linear gradient of 50 mM to 1 M NaCl in 20 column volumes. A DNA peak was eluted at 455 mM NaCl and a protein peak was eluted at 675 mM NaCl. Fractions containing the protein peak were pooled, and loaded onto a 116 ml (1.6 cm × 60 cm) Superose 12 (GE Healthcare) column equilibrated in 25 mM HEPES (pH 7.5); 50 mM NaCl and 1 mM DTT at 1 ml/min. Functional mRev1(1–131) eluted at 101 ml. An identical procedure was used to express and purify the N-terminally truncated mRev1 proteins and scRev1(1–251) which eluted at a volume of 77 ml.

Full-length and N-terminal truncated Rev1 proteins were prepared exactly as previously described [30].

**Table 1**
DNA sequences and secondary structures used in this study. Shaded residues indicate the hairpin structure and underlined residues indicate dsDNA. The DNA sequence is presented 5′–3′. All 5′ phosphate modifications were introduced enzymatically. The 3′ phosphate modification of 3′SHP was introduced upon synthesis.

| Name | Sequence | Structure |
|---|---|---|
| GAP0 | ACTCCACCC**TCAT**GGGTGGAGTCGTGTGAGC**TCAT**GCTCACACG | 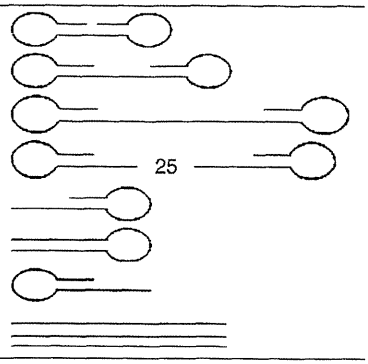 |
| GAP3 | ACTCCACCC**TCAT**GGGTGGAGTCTTGTGCTGGTG**TCAT**CACCAGCAC | |
| GAP10 | ACTCCACCC**TCAT**GGGTGGAGTCTTGTAATGAGTGTGGTCG**TCAT**CGACCACAC | |
| GAP25 | ACTCCACCC**TCAT**GGGTGGAGTGTTGGAGTGTTGTGAGGTTGGTTGGGTGTGGTCG**TCAT**CGACCACAC | |
| 5′SHP$_1$ | CTCGAGGTCG**TCAT**CGACCTCGAGATCA | |
| 5′SHP$_2$ | CTCGAGGTCG**TCAT**CGACCTCGAG | |
| 3′SHP | ACTGCTCGAGGTCG**TCAT**CGACCTCGAG | |
| ssDNA | TGGGGTGGGGT | |
| dsDNA | TGCAGATTGCGCAATCTGCA (self annealing) | |

### 2.4. Preparation of oligonucleotides

All oligonucleotides were commercially synthesized (Microsynth), and are presented in Table 1. For radiolabeling, 2 pmol of the selected DNA oligonucleotide was treated with T4 polynucleotide kinase (New England Biolabs) at 37 °C with 10 μCi (6000 Ci/mmol) $\gamma^{32}$P-ATP as a substrate. To ensure complete phosphorylation of the oligonucleotide, unlabeled ATP was added to a final concentration of 50 μM after 90 min of incubation and the reaction was continued for 30 min. For 3′ radiolabeling 2 pmol of the selected DNA oligonucleotide was treated with Klenow fragment (New England Biolabs) at 37 °C with 10 μCi (6000 Ci/mmol) a $^{32}$P-dCTP as a substrate.

To ensure a high percentage of base pairing, the hairpin oligonucleotides were denatured at 100 °C, and slowly cooled to room temperature. Unreacted radioactive nucleotides were removed using Sephadex G25 spin columns (GE Healthcare) following the standard protocol.

### 2.5. Electrophoretic Mobility Shift Assay (EMSA)

DNA binding was detected using a gel retardation (EMSA) assay. The indicated amount of protein was diluted in a buffer consisting of 10 mM HEPES, pH 7.8, 2 mM $MgCl_2$, 0.1 mM EDTA, 100 μg/ml bovine serum albumin, 15% glycerol, (0–1.6) μg/ml poly(dI-dC) (unless noted otherwise, Boehringer Mannheim) and 2 mM dithiothreitol in a total volume of 15 μl. 20 fmol of the $^{32}$P-labeled GAP3 oligonucleotide (see Table 1) in 5 μl was added, incubated on ice for 30 min, and applied to a non-denaturing 8% Tris–glycine acrylamide gel containing 2% glycerol. Electrophoresis was performed at 80 V for 20 min and subsequently 120 V for 40 min at 4 °C in 25 mM Tris–HCl pH 8.5, 200 mM glycine. The gel was dried and radioactivity was detected using X-Ray film (BioMax, Kodak).

For competition binding experiments, labeled and unlabeled oligonucleotides were premixed and then added to the protein solution. The ratio of the competing oligonucleotide to the radioactively labeled oligonucleotide in each assay is indicated in the figure legend. Radioactivity was detected using a phosphorimager (Biorad). For each reaction, the amount of protein–DNA complex was calculated as a percentage: percent bound = ([counts in shifted DNA]/[total counts per lane]) × 100. The competition efficiency was normalized and calculated from the percent bound by the following formula: (1 − [percent bound with specific competitor]/[percent bound without competitor]). A competition efficiency of 1 indicates that all of the $^{32}$P labeled oligonucleotide is replaced by the competitor in the protein–DNA complex.

### 2.6. Dephosphorylation assay

The indicated amount of protein was incubated on ice with 20 fmol of $^{32}$P GAP3 under the same conditions as the EMSA experiments in the absence of poly(dI-dC). Subsequently 3.33 units of calf intestinal phosphatase (CIP, New England Biolabs) were added to the reaction mixture which was further incubated on ice for the indicated amount of time and then analyzed using the EMSA. The gel was dried, and radioactivity was detected using X-Ray film (BioMax XAR, Kodak).

## 3. Results

### 3.1. Generation of expression constructs and purification

BRCT domains from a variety of proteins, including Rev1, have been shown to bind peptides phosphorylated by ATM or ATR [31]. In addition, the Rev1 BRCT domain may be involved in binding to PCNA [17]. The BRCT domain of mouse Rev1 encompasses amino acid residues 52–119, whereas the analogous residues in *Saccharomyces cerevisiae* Rev1 are 169–247. In both Rev1 proteins there is a region with unknown function, immediately N-terminal to the BRCT domain. Interestingly, this region may contain an α-helix as predicted by the PSIPRED secondary structure prediction server (Fig. 1A) [32]. We recently found a similar configuration for the BRCT region of RFC p140 and provided evidence that the α-helix N-terminal to the BRCT domain of RFC p140 is required for DNA binding, in addition to the BRCT domain itself [29]. This led us to speculate that the Rev1 BRCT region can also bind DNA. In order to investigate the binding properties of the BRCT region of Rev1 to phosphopeptides, PCNA and DNA, we generated constructs expressing the complete BRCT region of mouse Rev1 and yeast Rev1, including the BRCT domain and the N-terminal α-helix, fused to a C-terminal $his_6$-tag. The recombinant proteins are respectively referred to as mRev1(1–131) and scRev1(1–251) (Fig. 1B and C). In addition, two N-terminal truncations in the mouse Rev1 BRCT region were made based on the predicted secondary structure: (I) deletion of N-terminal residues up to the α-helix, resulting in mRev1(21–131), and (II) deletion of N-terminal residues including the α-helix N-terminal to the BRCT domain, resulting in mRev1(41–131) (Fig. 1B). All four proteins were expressed in *Escherichia coli* and subsequently purified using nickel affinity chromatography, ion exchange chromatography and gel filtration chromatography (see Supplementary information figures S1–S3). Importantly, this purification procedure results in a protein preparation that is free of contaminating DNA.

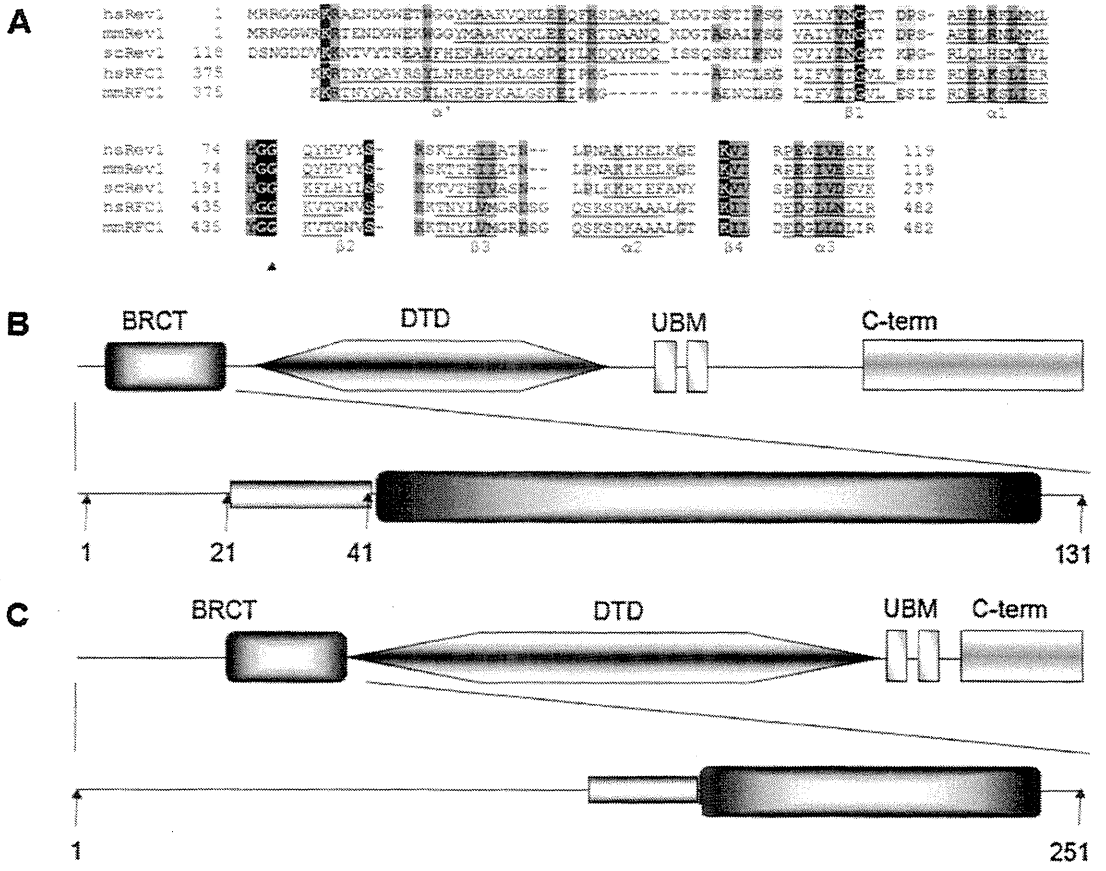


**Fig. 1.** (A) Amino acid sequence alignment of Rev1 and RFC p140 sequences generated by ClustalW. Residues with greater than 90% identity are shaded in black, 75% identity in dark grey and 50% identity in light grey. The secondary structure is indicated below the alignment. For the first 44 amino acids of mmRev1 and hsRev1 and the full scRev1 sequence the secondary structure was predicted using PSIPRED, for the other sequences the secondary structure is based on experimental data. (B) Domain composition of mmRev1, showing the BRCT domain (BRCT), the deoxycytidyl transferase domain (DTD), ubiquitin binding motifs (UBMs) and the C-terminal domain (C-term). The details of the BRCT region used in this study, including the position of the N-terminal α-helix, are shown below. (C) Domain composition of the analogous region of scRev1 with details of the BRCT region using in this study.

### 3.2. Mouse and yeast Rev1 bind DNA

To study DNA binding of the complete BRCT region of mouse Rev1, we titrated increasing amounts of protein into a $^{32}$P-labeled, double hairpin oligonucleotide containing a 3-nucleotide (nt) single stranded gap (5′P-GAP3, Table 1). Subsequently, DNA binding was analyzed using an EMSA. The oligonucleotide was based on the optimal substrate for structure-specific binding of the RFC p140 BRCT region but included an additional 3′ terminus to account for all possible common DNA structures. Migration of labeled 5′P-GAP3 was retarded in the presence of mRev1(1–131) indicating that this protein fragment binds the 5′P-GAP3 oligonucleotide (Fig. 2A). Quantitation of the DNA binding yielded an approximate $K_D$ of 160 nM (Fig. 2B), in comparison to approximately 10 nM for RFC p140(375–480) [29]. Similar results were found for the BRCT region of yeast Rev1 (Fig. 2C). To exclude the possibility that Rev1 BRCT binding to 5′P-GAP3 reflects a general DNA binding property of BRCT regions, we titrated an unrelated BRCT domain from human BRCA1 (aa 1646–1863) into a similarly labeled DNA. Even at protein to DNA ratios up to 2000:1 we could not observe any DNA binding (not shown). Furthermore, other biologically relevant *in vitro* DNA binding has been shown at similarly high ratios [33].

To further assess the relevance of DNA binding, we reevaluated the interaction of mRev1(1–131) with phosphopeptides and with PCNA (See Fig. S4). The former was done by competing binding to 5′P-GAP3 with a phosphopeptide library similar to that reported earlier [31]. No effect of the phosphopeptides on DNA binding was observed, using the EMSA. Since the highest ratio of phosphopeptide:DNA achievable was 37:1, it is possible to conclude that phosphopeptide binding, if present, is 5–10 times weaker than phospho DNA binding. Furthermore, NMR analysis of inorganic phosphate binding to mRev1(1–131) revealed only subtle changes in the spectrum of the protein suggesting at best an extremely weak interaction (not shown). Although it has been reported that the BRCT region of Rev1 binds PCNA *in vitro* [17], we were unable to detect binding of purified PCNA to immobilized mRev1(1–131) or *vice versa* (See Fig. S4). In conclusion, we find that the purified mouse Rev1 BRCT region preferentially binds to DNA rather than phosphopeptides or PCNA. For subsequent experiments aimed at delineating the specificity of the Rev1-DNA interaction we therefore focused on this protein fragment.

### 3.3. Specific DNA binding requires N-terminal amino acid residues in addition to the conserved BRCT domain

In our previous study of the BRCT region of RFC p140, DNA binding was dependent on a stretch of 28 residues N-terminal to the conserved BRCT domain [29]. To investigate whether the predicted α-helix of mRev1, N-terminal to the BRCT domain, plays a role in DNA binding, we assayed mRev1(1–131), mRev1(21–131) and mRev1(41–131) using the EMSA and the 5′P-GAP3 substrate (Fig. 3). At a protein:DNA ratio where mRev1(1–131) shifts nearly 100% of

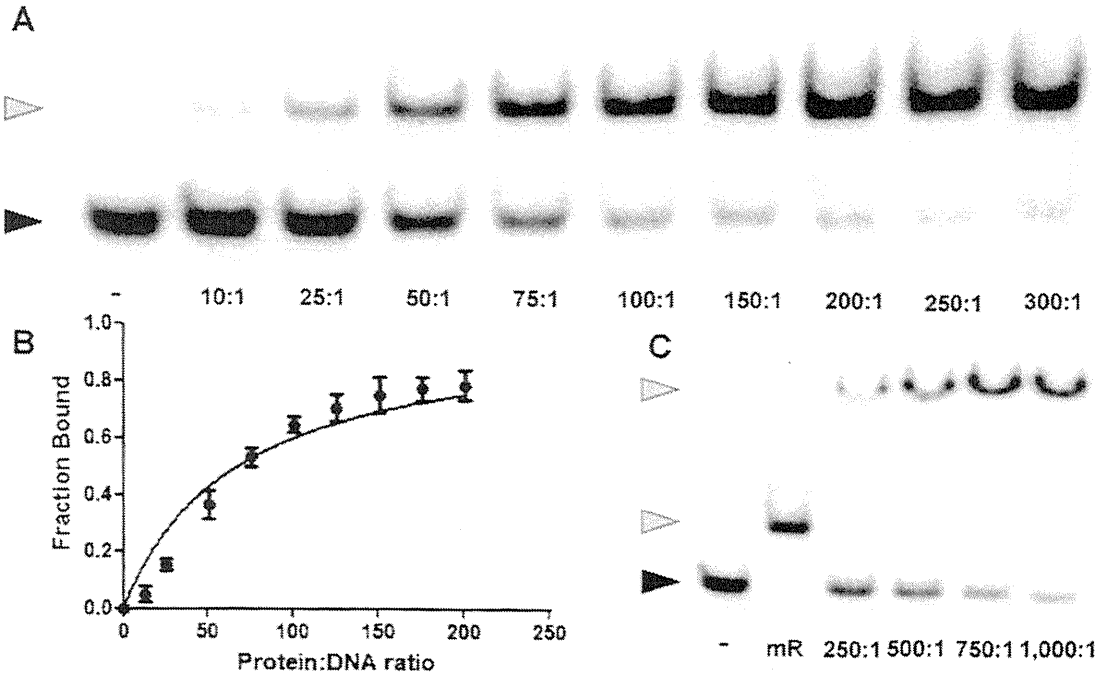


**Fig. 2.** DNA binding by the mouse and yeast Rev1 BRCT region. (A) mRev1(1–131) was titrated into a constant amount of $^{32}$P 5′ labeled GAP3 oligonucleotide (20 fmol) at the indicated ratios. The position of the DNA–protein complex is denoted by ⮞ and free DNA by ►. (B) The binding data in (A) were quantitated and fit to a single site binding curve to yield a $K_D$ of approximately 160 nM. (C) scRev1(1–131) was titrated into a constant amount of $^{32}$P labeled GAP3 oligonucleotide (20 fmol) at the indicated ratios. Lane marked "–" no protein, lane marked "mR" 6 pmol mRev1(1–131).

the input DNA, mRev1(21–131), which still contains the predicted N-terminal α-helix, bears considerably less DNA binding activity (compare Fig. 3A lane 1 vs. B lane 1). Additional removal of the N-terminal α-helix resulted in further loss of DNA binding (compare Fig. 3A lane 1 vs. C lane 1). To investigate DNA structure-specific vs. nonspecific dsDNA binding, we performed a competition experiment with poly(dI-dC) using different nucleotide ratios up to 3000:1 of poly(dI-dC):5′P-GAP3. Addition of poly(dI-dC) has a mod-

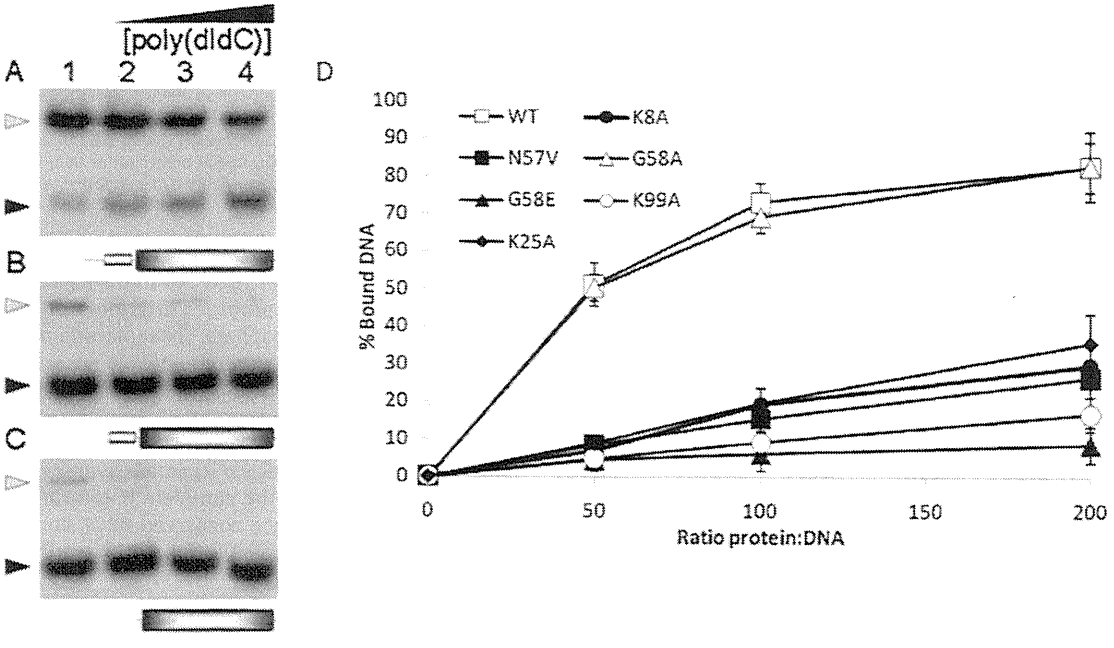


**Fig. 3.** The effect of N-terminal truncation on the DNA binding capability of the mouse Rev1 BRCT region. 16 pmol of the indicated protein was added to 20 fmol of $^{32}$P 5′ labeled GAP3 oligonucleotide, shown in the first lane of each gel. The contribution of non-specific dsDNA binding to complex formation was visualized by adding increasing amounts of poly(dI-dC) (respectively 0.23, 0.47, 0.80 μg/ml) during incubation, where 1 μg/ml corresponds to a nucleotide ratio of 3750:1 with respect to labeled DNA substrate. DNA–protein complex is denoted by ⮞ and free DNA by ►. Proteins are (A) mRev(1–131), (B) mRev(21–131) and (C) mRev(41–131), as shown schematically under each panel. (D) The effect of point mutations on DNA binding by mRev1(1–131). Respectively 2, 4 and 8 pmol of wild type or mutant mRev1(1–131) proteins was titrated into 20 fmol of 5′ phosphorylated GAP3. Free DNA and bound DNA were separated in a gel retardation assay. The intensity of the bands was determined using a phosphorimager and the percentage of bound DNA was calculated.

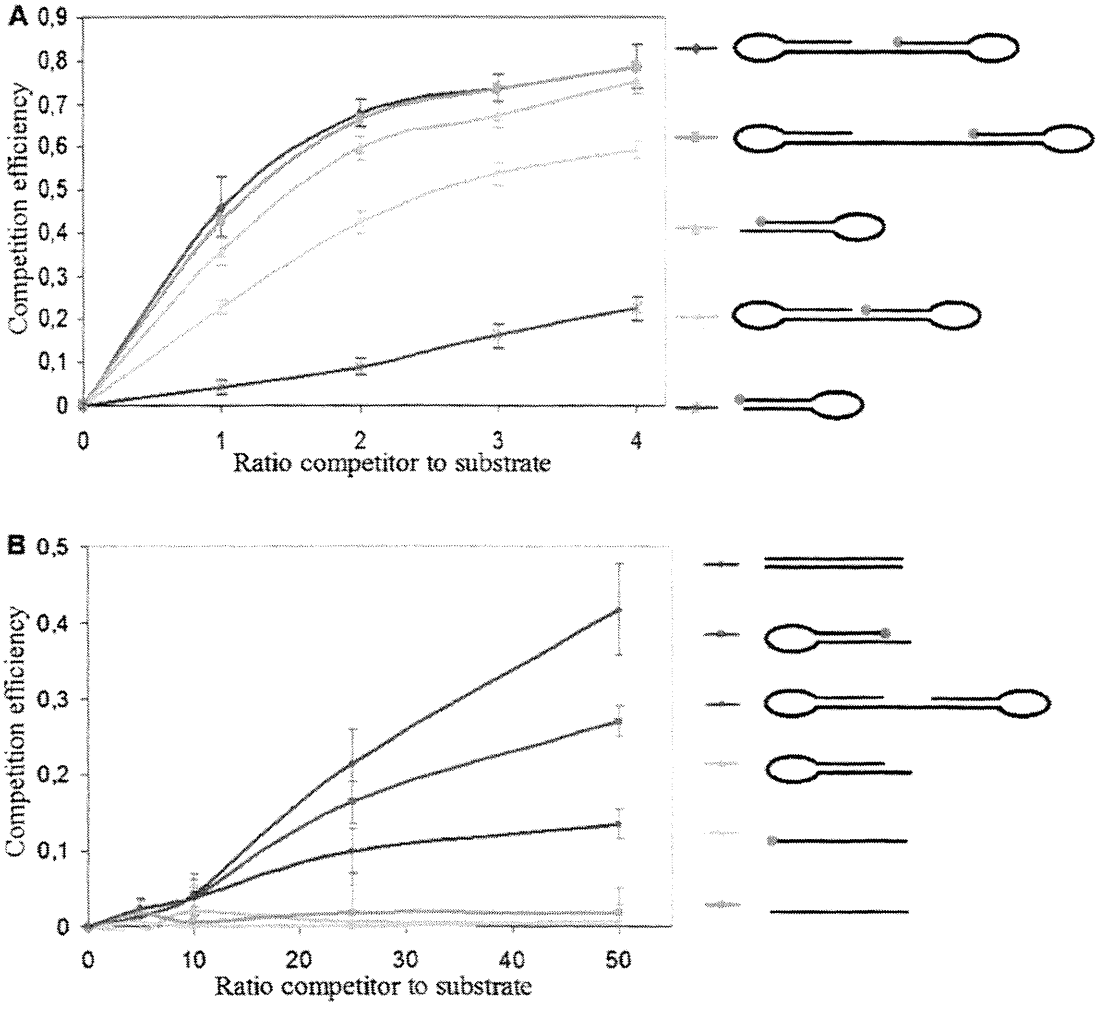


**Fig. 4.** Determination of structural features of the DNA substrate required for binding. (A) Different unlabeled 5′ phosphorylated DNA oligonucleotides were premixed with 20 fmol of $^{32}$P 5′ labeled GAP3 oligonucleotide at the indicated ratios and incubated with 6 pmol mRev1(1–131). The competition efficiency was determined by comparing binding of GAP3 in the presence of competitor to that in the absence of competitor. A competition efficiency of 1 indicates that all of the GAP3 DNA is displaced by the competitor DNA in the complex. Oligonucleotides used as competitors were respectively GAP3, GAP10, 5′ $SHP_1$, GAP0 and 5′ $SHP_2$ shown schematically on the right. The location of the 5′ phosphate is shown as a red dot. (B) Similar to (A) with the exception that the competitor DNA was titrated at higher ratios than in (A). The competitor oligonucleotides were respectively dsDNA, 3′ phosphorylated SHP (with 3′ phosphate indicated by a blue dot), unphosphorylated GAP3, 3′ SHP, 5′ phosphorylated ssDNA and ssDNA. See Table 1 for sequences of all nucleotides. Error bars represent the standard deviation of 5 separate datasets.

erate effect on DNA binding by mRev1(1–131) (Fig. 3A) suggesting that a small fraction of DNA binding is due to non-specific dsDNA binding. Residual DNA binding by both the mRev1(21–131) and mRev1(41–131) protein fragments was severely disrupted by the addition of poly(dI-dC) suggesting that the majority of DNA binding by these two protein fragments is non-specific to the DNA backbone.

We next investigated the role of specific amino acid residues in DNA binding. A series of point mutants was generated in mRev1(1–131) based on our previous work on RFCp140 [34]. The mutant proteins were purified and assayed for DNA binding using the EMSA (Fig. 3D). The mutants K8A and K25A from the N-terminal 20 residues and the predicted N-terminal α-helix respectively, both strongly reduce DNA binding confirming the results of Fig. 3B and C. Amino acid changes at N57 and K99 within the conserved BRCT domain, which are structurally analogous to the T415 and K458 of RFCp140, also strongly reduce DNA binding. The model of the RFCp140-DNA complex suggests that these residues are involved in 5′ phosphate recognition and the data in Fig. 3 are consistent with this possibility. In contrast, the G58A mutation had no effect on DNA binding by mRev1(1–131). In RFCp140 the backbone amide of the homologous residue was proposed to be involved in hydrogen bond formation with the 5′ phosphate. The replacement of a hydrogen by a methyl group in G58A is therefore likely not sufficient to disrupt interaction with the DNA. However, the introduction of a negative charge in the G58E mutant essentially abrogates DNA binding. This result suggests that indeed G58 is in close proximity to the DNA and may form hydrogen bonds *via* its amide hydrogen. Taken together these data suggest that the complete N-terminal BRCT region of mouse Rev1, including the conserved BRCT domain, plays a role in DNA binding which involves unique structural features of the 5′P-GAP3 substrate.

### *3.4. Structural features of DNA required for high affinity binding by mRev1(1–131)*

To investigate the DNA features required for high affinity binding by the BRCT region of mouse Rev1, we studied competition between $^{32}$P labeled 5′P-GAP3 and various unlabeled DNA oligonucleotides using the EMSA. The labeled 5′P-GAP3 and unla-

beled competing oligonucleotides were mixed prior to addition of mRev1(1–131). DNA binding was quantified using a phosphorimager and presented in graphic form as competition efficiency where a score of 1.0 means complete abolition of binding to the labeled substrate (Fig. 4). 5′P-GAP0, a 5′ phosphorylated double-hairpin oligonucleotide containing a nick rather than a ssDNA stretch, competed significantly less efficiently for binding mRev1(1–131) than 5′P-GAP3 (Fig. 4A), suggesting that ssDNA is important for mRev1(1–131) binding. The 10 nt ssDNA-containing GAP10 exhibited similar competition efficiency to 5′P-GAP3 itself, indicating that a ssDNA region longer than 3 nt has no stimulatory effect on binding by mRev1(1–131). Competition with a 5′ phosphorylated, single hairpin with a 3′ ssDNA overhang (5′P-$SHP_1$) is nearly as efficient as 5′P-GAP3 itself, suggesting only a minor effect of the 3′ dsDNA terminus on mRev1(1–131) binding. In further agreement with the requirement of a ssDNA stretch for mRev1(1–131) binding, 5′P-$SHP_2$, containing a hairpin and a blunt end, only competed weakly with binding of mRev1(1–131) to 5′P-GAP3.

In order to probe more subtle requirements for DNA binding of mRev1(1–131), we next investigated a series of substrates that were substantially less efficient competitors. Note that to achieve reasonable levels of competition it was necessary to titrate these substrates to a roughly 10 fold greater ratio to 5′P-GAP3 (Fig. 4B) than those depicted in Fig. 4A. Consistent with the results of the poly(dI-dC) titration, addition of blunt ended, non-phosphorylated 20 base pair (bp) dsDNA competed, albeit weakly, with 5′P-GAP3. The competition efficiency of the non-phosphorylated 20 bp oligonucleotide was greater than that of non-5′ phosphorylated GAP3 while a non-phosphorylated SHP oligonucleotide with a 10 bp dsDNA region failed to elicit any competition. This suggests a requirement for a stretch of contiguous dsDNA longer than 10 bp for optimal binding. A 3′ phosphorylated single hairpin (3′P-SHP) also weakly competed with 5′P-GAP3 for mRev1(1–131) binding. Neither non-phosphorylated ssDNA nor 5′ phosphorylated ssDNA resulted in detectable competition with the labeled GAP3 substrate, even at a 50:1 ratio. Together these results demonstrate that the BRCT region of mouse Rev1 preferentially binds to the recessed, 5′ phosphorylated end of a primer–template junction.

### 3.5. The Rev1 BRCT region – DNA complex has a long lifetime in vitro

To study the stability of the interaction between the mRev1 BRCT region and a recessed phosphorylated 5′ end of a gapped substrate, we determined exchange kinetics. First, we performed a time course analysis of competition binding using the EMSA (Fig. 5A). We pre-incubated mRev1(1–131) with unlabeled 5′P-GAP3 for 30 min. We then challenged the complex with $^{32}$P labeled 5′P-GAP3 for various periods of time. Fig. 5A shows that at short time periods only a small amount of the unlabeled DNA was displaced by the labeled DNA. However, after 30 min equilibrium was reached as the amount of labeled molecules in protein–DNA complexes was equal to that when $^{32}$P labeled 5′P-GAP3 was pre-mixed with unlabeled DNA (Fig. 5A, lanes 5 and 6). This result indicates that the dissociation of the protein fragment from its substrate may be a slow process. To specifically investigate the dissociation rate from the 5′ phosphate, we investigated the sensitivity of the 5′ $^{32}$P to phosphatase treatment after mixing the protein and DNA. In this assay naked 5′ $^{32}$P GAP3 is almost completely dephosphorylated within the time required for the DNA to enter the gel, resulting in complete loss of the labeled signal (Fig. 5B). In contrast, after pre-incubation with mRev1(1–131), phosphorylated 5′P-GAP3 is still observable even after 15 min of phosphatase treatment. Thus, the dissociation rate of mRev1(1–131) from a recessed 5′ phosphorylated primer–dimer junction is very slow, with a half life of 5–7 min. A similar experiment was performed using mRev1(21–131) under

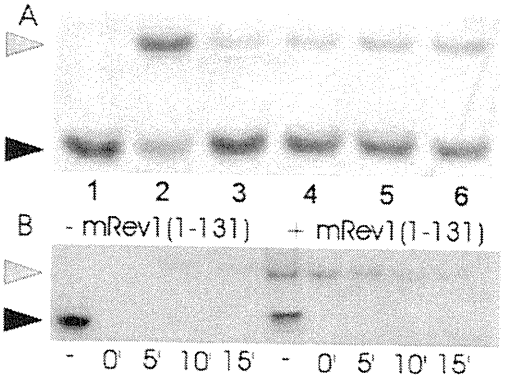


**Fig. 5.** mRev1(1–131) releases 5′-phosphorylated DNA with slow kinetics. (A) Time-dependent binding of $^{32}$P GAP3 by mRev1(1–131). Lane 1, no protein added. Lane 2, mRev1(1–131):$^{32}$P GAP3-complex at a ratio of 400:1. Lanes 3–5, 5′-$^{32}$P GAP3 was added for 5′, 15′ or 30′ respectively at an equimolar ratio to unlabeled GAP3 that was preincubated for 30′ with mRev(1–131). Lane 6, equimolar ratio of labeled and unlabeled GAP3 were both preincubated with mRev1(1–131) for 30′. (B) DNA binding by mRev1(1–131) protects the 5′ phosphate from phosphatase treatment. mRev1(1–131), or mock assay without protein, was incubated with 5′-$^{32}$P GAP3 at a ratio of 400:1 for 30 min. Subsequently, calf intestinal phosphatase was added for the indicated time before gel electrophoresis. The control reactions show that phosphatase treatment was complete before the DNA enters the gel. DNA–protein complex is denoted by ⊱ and free DNA by ►.

conditions where approximately 20% of the $^{32}$P labeled 5′P-GAP3 was bound. We could not detect any protection from phosphatase, further suggesting that the N-terminal 20 aa are required for high affinity DNA binding (not shown). Together these experiments suggest that the binding of the Rev1 BRCT region to a 5′ phosphorylated DNA end is stable.

### 3.6. Full-length Rev1 binds to both 5′ phosphorylated and 3′ OH ends of primer–template junctions

To investigate whether the preferential binding properties of the isolated Rev1 BRCT region are indicative of those of the full length Rev1 protein, we assayed the DNA substrate specificities of full length mRev1 [mRev1(1–1249)] and of truncated mRev1 proteins that contain N-terminal deletions similar to those introduced in the isolated BRCT region [mRev1(21–1249) and mRev1(41–1249)]. As substrate we used 5′P-$SHP_1$, containing a 5′ P primer–template junction, to which mRev1(1–131) bound with good efficiency (Table 1, Fig. 4A). While mRev1(1–131) and mRev1(1–1249), both of which contain the entire BRCT region, efficiently bound the 5′P-$SHP_1$ substrate, neither of the N-terminally truncated proteins mRev1(21–1249) and mRev1(41–1249) exhibited any DNA binding activity (Fig. 6A). When we assessed binding to a recessed 3′ OH terminus using the 3′ $SHP_1$ oligonucleotide (Table 1, Fig. 6A), all Rev1 fragments bound, with the exception of mRev1(1–131). This suggests that portions of the protein, C-terminal to the BRCT region, are required for binding to this substrate. These data indicate that the BRCT region is exclusively involved in binding a recessed 5′ phosphorylated primer–template junction whereas amino acid residues C-terminal to residue 131 of mRev1 direct specific binding to a recessed 3′ primer–template junction (Fig. 6A). We next assayed double hairpin substrates with a 25 nucleotide gap (GAP25) (Fig. 6B). This oligonucleotide with a larger single-stranded gap was chosen to avoid steric hindrance should the rather large Rev1 bind at both the 5′ and 3′ termini. In agreement with the data in Fig. 6A, mRev1(1–1249) as well as the N-terminally truncated mRev1 protein fragments bound GAP25 containing a non-phosphorylated 5′ terminus, while mRev1(1–131) did not bind. However, all four protein fragments bind a GAP25 substrate containing both a 3′ OH and a 5′ P terminus (5′P-GAP25, Fig. 6B). Although in principle one might

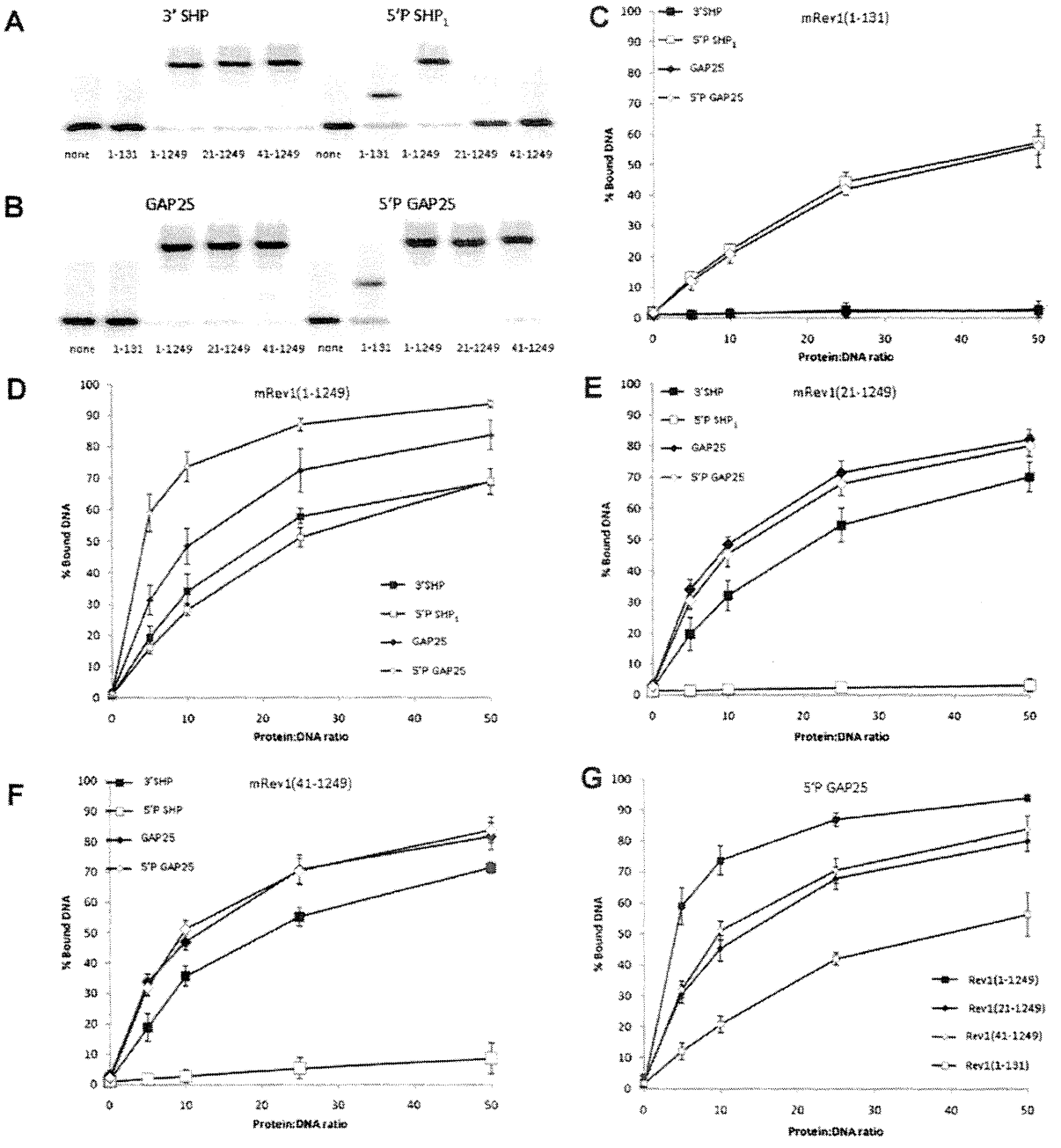


**Fig. 6.** DNA binding by full length Rev1. (A) mRev1(1–131), mRev1(1–1249), mRev1(21–1249) and mRev1(41–1249) were added to $^{32}$P labeled 3′ SHP or 5′ SHP$_1$ substrate at a ratio of 50:1. (B) mRev1(1–131), mRev1(1–1249), mRev1(21–1249) and mRev1(41–1249) were added to $^{32}$P labeled GAP25 3′ OH or GAP25 5′ Phos substrate at a ratio of 50:1. (C–F) Quantification of three independent EMSAs in which respectively mRev1(1–131) (C), mRev1(1–1249) (D), mRev1(21–1249) (E), and mRev1(41–1249) (F) were titrated into a constant amount of the indicated DNA substrate. (G) Comparison of results from (C–F) to visualize the differences between respectively full length mRev1, mRev1(21–1249), mRev1(41–1249) and mRev1(1–131) with respect to binding of the 5′ phosphorylated GAP25.

expect that one molecule of Rev1 could bind to the 5′ P and a second one to the 3′ OH, the data suggest that the stoichiometry is predominantly, if not exclusively, 1:1 (see Fig. S5 for an enlargement of the full gel and explanation).

To further characterize the difference in DNA binding by the various Rev1 protein fragments, increasing amounts of each fragment were titrated into the indicated DNA substrates and DNA binding was quantified (Fig. 6C–G). In line with our previous results, mRev1(1–131) binds only 5′P-SHP$_1$ and 5′P-GAP25 (Figs. 4A and 6C). mRev1(1–1249) binds the 3′ SHP and 5′P-SHP$_1$ substrates with comparable affinities and displays a slightly higher affinity for unphosphorylated GAP25. The DNA binding affinity for 5′P-GAP25 was highest, suggesting binding of mRev1(1–1249) to both recessed 5′ phosphorylated, and 3′ primer-template junctions (Fig. 6D). Both mRev1(21–1249) and mRev1(41–1249) also show a slightly higher binding affinity for unphosphorylated GAP25 in comparison to 3′ SHP, but the increased binding affinity for a 5′P-GAP25 is not observed (Fig. 6E and F). The binding affinity for 5′P-GAP25 is in the order mRev1(1–131) < mRev1(21–1249) = mRev1(41–1249) < mRev1(1–1249) (Fig. 6G). Combined, these results suggest that, akin to the isolated Rev1 BRCT region, the BRCT region in full-length mRev1 is essential for binding of mRev1 to the recessed, 5′ phosphorylated end of a primer-template junction.

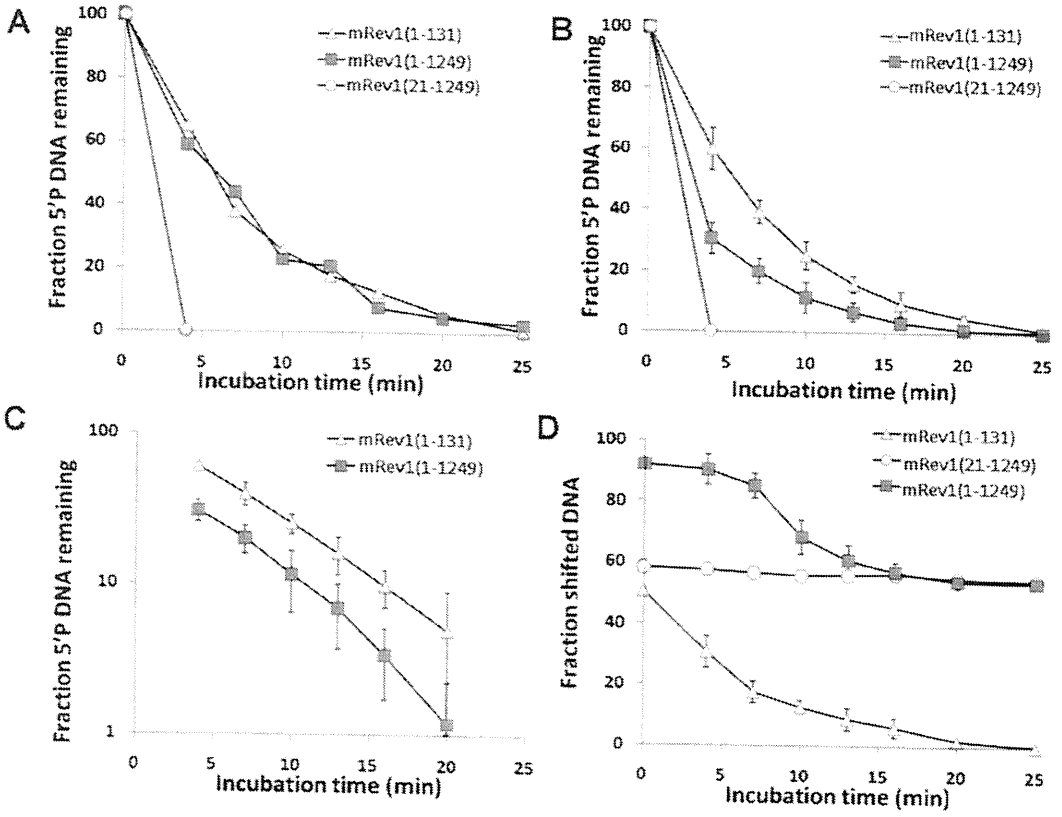


**Fig. 7.** Protection of the 5′ phosphate is maintained in full-length mRev1. (A) mRev1(1–131), mRev1(1–1249) and mRev1(21–1249) were incubated with phosphorylated 5′ $SHP_1$ for 30 min. Subsequently, calf intestinal phosphatase was added for the indicated time before running the gel. (B) Similar experiment as in (A) with respectively mRev1(1–131), mRev1(1–1249) and mRev1(21–1249) incubated with 5′ labeled 5′ phosphorylated GAP25. (C) Data from figure B plotted on logarithmic scale. (D) Similar experiment as in (B) and (C) with 3′ labeled 5′ phosphorylated GAP25.

Next we asked whether the DNA binding kinetics, observed in the isolated BRCT region, were retained in the context of the full-length protein. Thus, mRev1(1–131), mRev1(1–1249) and mRev1(21–1249) were preincubated with $^{32}P$ labeled 5′P-$SHP_1$ and subsequently subjected to phosphatase treatment (Fig. 7A), similar to the experiment depicted in Fig. 5B. When mRev1(21–1249) was preincubated with $^{32}P$ labeled 5′ $SHP_1$, the DNA was completely dephosphorylated within the time required for the DNA to enter the gel, whereas both mRev1(1–131) and mRev1(1–1249) displayed a identical protective effect against dephosphorylation of 5′ $SHP_1$ (Fig. 7A), confirming the slow release from a recessed 5′ primer terminus (see above). When the experiment was repeated with 5′P-GAP25 as a substrate, mRev1(1–1249) initially showed a faster release from the 5′ phosphate than mRev1(1–131) but subsequently the release was similar (Fig. 7B and C). This initial faster release may be explained by binding of mRev1(1–1249) to either the 5′ or 3′ termini, leaving a greater portion of 5′ termini unprotected. To test whether dephosphorylation of 5′P-GAP25 affects DNA binding of mRev1(1–131), mRev1(1–1249) and mRev1(21–1249), we repeated the experiment using 5′P-GAP25 substrate that was labeled by incorporation of an $\alpha$-$^{32}P$ nucleotide at the 3′ terminus using Klenow fragment (Fig. 7D). This labeling is refractory to phosphatase treatment, allowing an analysis of protein–DNA binding, even after removal of the 5′ P. The rate of loss of DNA binding by mRev1(1–131) is the same as the rate of loss of $^{32}P$ label (Fig. 7D) confirming that binding of this protein fragment is entirely dependent on the 5′ P at the primer–template junction. In contrast, mRev1(21–1249) stably binds a smaller fraction of the input DNA. Since this binding is entirely independent of the loss of 5′ P, this result suggests that mRev(21–1249) stably associates with the 3′ OH terminus of the DNA. Full length mRev1(1–1249) however, exhibits a very different behavior. mRev1(1–1249) binds nearly all of the input DNA and undergoes an initial slow loss of DNA binding upon phosphatase treatment. After approximately 15 min of phosphatase treatment, DNA binding by mRev1(1–1249) reaches a plateau that precisely matches that of mRev1(21–1249). The additional binding, compared to mRev1(21–1249), and slow release upon phosphatase treatment suggests that initially either the 3′ OH or the 5′ P terminus is bound by mRev1(1–1249). Since the 5′ P is released relatively rapidly (Fig. 7B), the slow release from 3′ labeled GAP25 indicates that Rev1, after release from the 5′ P, transiently remains tethered to the single-stranded region before releasing the DNA. These results confirm that the BRCT region of full length Rev1 preferentially binds to phosphorylated 5′ termini of gapped substrates. Independent of the BRCT region, other portions of Rev1 are important for stable binding to 3′ termini.

## 4. Discussion

Here we present evidence that the BRCT region of mammalian and yeast Rev1 protein displays a highly specific interaction with a recessed, 5′ phosphorylated terminus of a double-stranded DNA molecule. We also show that other portions of mRev1 are important for binding at the 3′ OH terminus of the molecule, and transiently to single-stranded DNA, consistent with previous studies [28]. The interaction with a recessed, 5′ phosphorylated primer–template terminus requires the complete BRCT region, including the conserved BRCT domain, the N-terminal 20 amino acids and the predicted $\alpha$-helix. Preliminary NMR analysis of the different mouse Rev1 proteins used in this study suggests that the first 20 amino acids are completely unfolded (not shown), an observation that

is consistent with the PSIPRED prediction of the total absence of any secondary structure. DNA binding is not uncommon for BRCT domains. In addition to our work on the BRCT region of RFC p140, BRCT domains have been implicated in direct DNA binding of X family polymerases [35] and of bacterial NAD(+) dependent ligases [36,37]. The BRCT domain of the bacterial NAD(+) dependent ligases binds both dsDNA and ssDNA, while the specificity of both the Rev1 and RFC p140 BRCT region is clearly for recessed, phosphorylated 5′ ends in dsDNA.

Amongst the various DNA binding BRCT domains studied so far, the BRCT region of Rev1 is the only one showing slow binding kinetics. The slow off rate results in a protein–DNA complex that sterically blocks access to the 5′ phosphate with a half life of about 5–7 min. The measured affinity and $k_{off}$ suggest a $k_{on}$ on the order of $10^4\ s^{-1}$ (where $K_D = k_{off}/k_{on}$), five orders of magnitude slower than diffusion-limited binding. A possible explanation for the slow on rate is that high affinity binding to the 5′ phosphate requires folding of the N-terminal 20 aa, which could be rate limiting.

In contrast to previous studies [17,31], we did not find evidence for binding of the mRev1 BRCT region to phosphopeptides, nor to PCNA. Possibly the observed co-immunoprecipitation of the Rev1 BRCT domain with PCNA is mediated *via* their common binding to DNA. Our observations during the purification of the various Rev1 proteins used in this study are that significant amounts of DNA copurify during metal affinity and size exclusion chromatography, which is separated from the protein only after cation exchange chromatography.

We found that, in addition to the N-terminal BRCT region that directs binding of mRev1 to a recessed, 5′ phosphorylated primer–template junction, other portions of the protein mediate mRev1 binding to the 3′ OH terminus of the gap. Interestingly, binding at the 3′ OH, but not at the 5′ phosphate, is dependent on the length of the ssDNA (compare binding of 3′ SHP with binding of GAP25 in Fig. 6). A possible explanation is the reported ssDNA binding property of the polymerase domain region [27,28], which may slightly increase the affinity for the gapped substrate in comparison to the single hairpin substrate. The affinity of mRev1(1–1249) for a 5′ phosphorylated gapped DNA is significantly greater than for a non-phosphorylated DNA, while the stoichiometry remains unchanged as judged by migration in the EMSA. This suggests that in our assay mRev1(1–1249) binds to either end of the DNA compared with mRev1(21–1249) that only binds at the recessed 3′ primer–template junction (Fig. 6B). While the reason for the 1:1 stoichiometry is not clear, the flexibility and length of the single-stranded gap in principle allow either two Rev1 molecules to simultaneously bind or a single Rev1 to bind both termini.

We have also shown that binding of both mRev1(1–131) and mRev1(1–1249) to a 5′ phosphorylated primer–template junction protects it from dephosphorylation. Interestingly, following removal of the 5′ phosphate, mRev1(1–1249) did not immediately dissociate but remained transiently bound to the DNA (Fig. 7D). In contrast, mRev1(1–131) releases dephosphorylated DNA with the same kinetics as the dephosphorylation itself. In the crystal structure, the dCMP transferase domain of human Rev1 encircles the DNA [38]. If 5′ phosphate binding allows this "loading" of the dCMP transferase domain onto the upstream ssDNA, then the topological restriction could explain the transient association. Of note, it was previously found that Rev1 displays single-strand DNA translocase activity *in vitro* [28]. The observed translocase activity is in agreement with the transient binding of full-length Rev1 to the gap-containing oligonucleotide after release of the protein from the 5′ phosphorylated primer–template junction.

The *in vitro* interaction of the Rev1 BRCT region with a 5′ phosphorylated primer at a primer–template junction may have relevance for understanding the function of the protein during TLS *in vivo*. In mammalian cells, recruitment of Rev1 to foci that presumably represent replication forks stalled at endogenous DNA damage, depends on the BRCT domain [17]. Furthermore, an error-prone DNA TLS pathway that operates early after UV treatment also depends on the Rev1 BRCT region [21]. These data support the relevance of the domain for TLS in mammals, although in Rev1-deficient chicken DT40 cells complemented with an ectopically expressed Rev1 BRCT deletion mutant, TLS was not affected [7,22]. Recent studies have shown that in *S. cerevisiae* TLS can take place at post-replicative single-strand gaps opposing the fork-blocking lesion [25,26]. Also, in mammalian cells Rev1 deficiency leads to the accumulation of post-replicative gaps opposite helix-distorting photolesions [21]. In this context it is conceivable that Rev1, *via* its BRCT region, is recruited to a free 5′-phosphorylated primer–template junction flanking a single-strand DNA gap, downstream of the fork-arresting lesion. Such a mode of recruitment restricts the mutagenic activity of Rev1 to post-replicative TLS at severely distorting, mutagenic, DNA lesions [21,27], thereby preventing the inadvertent recruitment of the mutagenic TLS machinery to a processive replication fork.

## Conflict of interest

None.

## Acknowledgement

The authors are indebted to Dr. Jan Wouter Drijfhout of the Leiden University Medical Center for preparation of the phosphopeptide library.

## Appendix A. Supplementary data

Supplementary data associated with this article can be found, in the online version, at doi:10.1016/j.dnarep.2011.04.033.

## References

[1] L.S. Waters, B.K. Minesinger, M.E. Wiltrout, S. D'Souza, R.V. Woodruff, G.C. Walker, Eukaryotic translesion polymerases and their roles and regulation in DNA damage tolerance, Microbiol. Mol. Biol. Rev. 73 (2009) 134–154.
[2] M.D. Sutton, G.C. Walker, Managing DNA polymerases: coordinating DNA replication, DNA repair, and DNA recombination, Proc. Natl. Acad. Sci. U.S.A. 98 (2001) 8342–8349.
[3] C.W. Lawrence, Cellular functions of DNA polymerase zeta and Rev1 protein, DNA Repair Replicat. 69 (2004) 167–203.
[4] J.R. Nelson, C.W. Lawrence, D.C. Hinkle, Deoxycytidyl transferase activity of yeast REV1 protein, Nature 382 (1996) 729–731.
[5] C. Otsuka, N. Kunitomi, S. Iwai, D. Loakes, K. Negishi, Roles of the polymerase and BRCT domains of Rev1 protein in translesion DNA synthesis in yeast in vivo, Mutat. Res.-Fund. Mol. Mech. Mutagen. 578 (2005) 79–87.
[6] X.J. Lin, T. Okuda, J. Trang, S.B. Howell, Human REV1 modulates the cytotoxicity and mutagenicity of cisplatin in human ovarian carcinoma cells, Mol. Pharmacol. 69 (2006) 1748–1754.
[7] A.L. Ross, L.J. Simpson, J.E. Sale, Vertebrate DNA damage tolerance requires the C-terminus but not BRCT or transferase domains of REV1, Nucleic Acids Res. 33 (2005) 1280–1289.
[8] J.R. Nelson, P.E.M. Gibbs, A.M. Nowicka, D.C. Hinkle, C.W. Lawrence, Evidence for a second function for *Saccharomyces cerevisiae* Rev1p, Mol. Microbiol. 37 (2000) 549–554.
[9] C.X. Guo, P.L. Fischhaber, M.J. Luk-Paszyc, Y. Masuda, J. Zhou, K. Kamiya, C. Kisker, E.C. Friedberg, Mouse Rev1 protein interacts with multiple DNA polymerases involved in translesion DNA synthesis, EMBO J. 22 (2003) 6621–6630.
[10] A. Wood, P. Garg, P.M.J. Burgers, A ubiquitin-binding motif in the translesion DNA polymerase Rev1 mediates its essential functional interaction with ubiquitinated proliferating cell nuclear antigen in response to DNA damage, J. Biol. Chem. 282 (2007) 20256–20263.
[11] C.X. Guo, T.S. Tang, M. Bienko, J.L. Parker, A.B. Bielen, E. Sonoda, S. Takeda, H.D. Ulrich, I. Dikic, E.C. Friedberg, Ubiquitin-binding motifs in REV1 protein are required for its role in the tolerance of DNA damage, Mol. Cell. Biol. 26 (2006) 8892–8900.
[12] I. Callebaut, J.P. Mornon, From BRCA1 to RAP1: a widespread BRCT module closely associated with DNA repair, FEBS Lett. 400 (1997) 25–30.

[13] P. Bork, K. Hofmann, P. Bucher, A.F. Neuwald, S.F. Altschul, E.V. Koonin, A superfamily of conserved domains in DNA damage-responsive cell cycle checkpoint proteins, FASEB J. 11 (1997) 68–76.
[14] J.N.M. Glover, R.S. Williams, M.S. Lee, Interactions between BRCT repeats and phosphoproteins: tangled up in two, Trends Biochem. Sci. 29 (2004) 579–585.
[15] J.F. Lemontt, Mutants of yeast defective in mutation induced by ultraviolet light, Genetics 68 (1971) 21.
[16] J.G. Jansen, A. Tsaalbi-Shtylik, P. Langerak, F. Calleja, C.M. Meijers, H. Jacobs, N. de Wind, The BRCT domain of mammalian Rev1 is involved in regulating DNA translesion synthesis, Nucleic Acids Res. 33 (2005) 356–365.
[17] C.X. Guo, E. Sonoda, T.S. Tang, J.L. Parker, A.B. Bielen, S. Takeda, H.D. Ulrich, E.C. Friedberg, REV1 protein interacts with PCNA: significance of the REV1 BRCT domain in vitro and in vivo, Mol. Cell 23 (2006) 265–271.
[18] S. D'Souza, G.C. Walker, Novel role for the C terminus of *Saccharomyces cerevisiae* Rev1 in mediating protein–protein interactions, Mol. Cell. Biol. 26 (2006) 8173–8182.
[19] A. Tissier, P. Kannouche, M.P. Reck, A.R. Lehmann, R.P. Fuchs, A. Cordonnier, Co-localization in replication foci and interaction of human Y-family members, DNA polymerase pol eta and REV1 protein, DNA Repair 3 (2004) 1503–1514.
[20] Y. Hirano, K. Sugimoto, ATR homolog Mec1 controls association of DNA polymerase zeta-Rev1 complex with regions near a double-strand break, Curr. Biol. 16 (2006) 586–590.
[21] J.G. Jansen, A. Tsaalbi-Shtylik, G. Hendriks, H. Gali, A. Hendel, F. Johansson, K. Erixon, Z. Livneh, L.H.F. Mullenders, L. Haracska, N. de Wind, Separate domains of Rev1 mediate two modes of DNA damage bypass in mammalian cells, Mol. Cell. Biol. 29 (2009) 3113–3123.
[22] C.E. Edmunds, L.J. Simpson, J.E. Sale, PCNA ubiquitination and REV1 define temporally distinct mechanisms for controlling translesion synthesis in the avian cell line DT40, Mol. Cell 30 (2008) 519–529.
[23] M. Lopes, M. Foiani, J.M. Sogo, Multiple mechanisms control chromosome integrity after replication fork uncoupling and restart at irreparable UV lesions, Mol. Cell 21 (2006) 15–27.
[24] A.R. Lehmann, R.P. Fuchs, Gaps and forks in DNA replication: rediscovering old models, DNA Repair 5 (2006) 1495–1498.
[25] Y. Daigaku, A.A. Davies, H.D. Ulrich, Ubiquitin-dependent DNA damage bypass is separable from genome replication, Nature 465 (2010) 951–955.
[26] G.I. Karras, S. Jentsch, The RAD6 DNA damage tolerance pathway operates uncoupled from the replication fork and is functional beyond S phase, Cell 141 (2010) 255–267.
[27] J.G. Jansen, M.I. Fousteri, N. de Wind, Send in the clamps: control of DNA translesion synthesis in eukaryotes, Mol. Cell 28 (2007) 522–529.
[28] Y. Masuda, K. Kamiya, Role of single-stranded DNA in targeting REV1 to primer termini, J. Biol. Chem. 281 (2006) 24314–24321.
[29] M. Kobayashi, F. Figaroa, N. Meeuwenoord, L.E.T. Jansen, G. Siegal, Characterization of the DNA binding and structural properties of the BRCT region of human replication factor C p140 subunit, J. Biol. Chem. 281 (2006) 4308–4317.
[30] Y. Masuda, M. Takahashi, S. Fukuda, M. Sumii, K. Kamiya, Mechanisms of dCMP transferase reactions catalyzed by mouse Rev1 protein, J. Biol. Chem. 277 (2002) 3040–3046.
[31] X. Yu, C.C.S. Chini, M. He, G. Mer, J.J. Chen, The BRCT domain is a phospho-protein binding domain, Science 302 (2003) 639–642.
[32] L.J. McGuffin, K. Bryson, D.T. Jones, The PSIPRED protein structure prediction server, Bioinformatics 16 (2000) 404–405.
[33] L.T. Yang, J.R. Mullen, S.J. Brill, Purification of the yeast Slx5–Slx8 protein complex and characterization of its DNA-binding activity, Nucleic Acids Res. 34 (2006) 5541–5551.
[34] M. Kobayashi, A.B. Eiso, A.M.J.J. Bonvin, G. Siegal, Structure of the DNA-bound BRCA1 C-terminal region from human replication factor C p140 and model of the protein–DNA complex, J. Biol. Chem. 285 (2010) 10087–10097.
[35] Y.M. Ma, H.H. Lu, B. Tippin, M.F. Goodman, N. Shimazaki, O. Koiwai, C.L. Hsieh, K. Schwarz, M.R. Lieber, A biochemically defined system for mammalian nonhomologous DNA end joining, Mol. Cell 16 (2004) 701–713.
[36] H. Feng, J.M. Parker, J. Lu, W.G. Cao, Effects of deletion and site-directed mutations on ligation steps of NAD(+)-dependent DNA ligase: a biochemical analysis of BRCA1 C-terminal domain, Biochemistry 43 (2004) 12648–12659.
[37] A. Wilkinson, A. Smith, D. Bullard, M. Lavesa-Curto, H. Sayer, A. Bonner, A. Hemmings, R. Bowater, Analysis of ligation and DNA binding by *Escherichia coli* DNA ligase (LigA), Biochim. Biophys. Acta Proteins Proteomics 1749 (2005) 113–122.
[38] M.K. Swan, R.E. Johnson, L. Prakash, S. Prakash, A.K. Aggarwal, Structure of the human Rev1–DNA–dNTP ternary complex, J. Mol. Biol. 390 (2009) 699–709.